Quantum dynamics of laser-induced desorption from metal and semiconductor surfaces, and related phenomena

2006 J. Phys.: Condens. Matter 18 S1425

(http://iopscience.iop.org/0953-8984/18/30/S05)

INSTITUTE OF PHYSICS PUBLISHING JOURNAL OF PHYSICS: CONDENSED MATTER

J. Phys.: Condens. Matter **18** (2006) S1425–S1459 doi:10.1088/0953-8984/18/30/S05

Quantum dynamics of laser-induced desorption from metal and semiconductor surfaces, and related phenomena

Peter Saalfrank, Mathias Nest, Ivan Andrianov, Tillmann Klamroth, Dominik Kröner and Stephanie Beyvers

Universität Potsdam, Institut für Chemie, Theoretische Chemie, Karl-Liebknecht-Straße 24-25, D-14476 Potsdam-Golm, Germany

Received 9 January 2006, in final form 23 March 2006
Published 14 July 2006
Online at stacks.iop.org/JPhysCM/18/S1425

Abstract

Recent progress towards a quantum theory of laser-induced desorption and related phenomena is reviewed, for specific examples. These comprise the photodesorption of NO from Pt(111), the scanning tunnelling microscope and laser-induced desorption and switching of H at Si(100), and the electron stimulated desorption and dissociation of CO at Ru(0001). The theoretical methods used for nuclear dynamics range from open-system density matrix theory over nonadiabatically coupled multi-state models to electron–nuclear wavepackets. Also, aspects of time-dependent spectroscopy to probe ultrafast nonadiabatic processes at surfaces will be considered for the example of two-photon photoemission of solvated electrons in ice layers on Cu(111).

(Some figures in this article are in colour only in the electronic version)

Dedicated to Professor Volker Staemmler on the occasion of his 65th birthday.

1. Introduction

1.1. Photoreactions at surfaces

The desorption of adspecies from solid surfaces is a key reaction in heterogeneous catalysis, photocatalysis, and surface nanochemistry [1, 2]. Photodesorption with UV/visible light, the simplest of all photoreactions at surfaces, is also interesting as a prototypical example for a wider class of nonadiabatic processes [3]. With light, a number of other surface reactions can be initiated such as photodissociation [4], photoassociation [5], photodiffusion [6, 7], and more complex photoreactions [8], with potential implications for molecular machines [9], rotors [10], and switches [11].

Photodesorption can be enforced either *directly*, or *indirectly*. In the first case photons couple directly to the dipole moment of the adsorbate–substrate complex. Direct coupling is

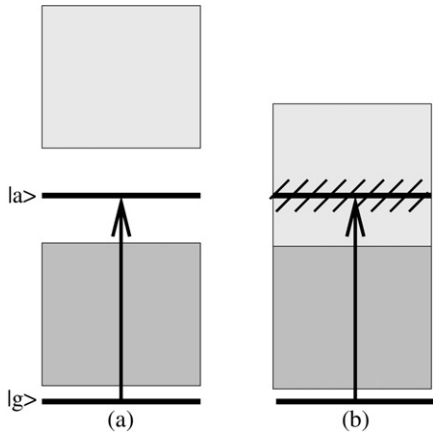

Figure 1. Illustration of the optical excitation of an adsorbate state $|a\rangle$ from an initial state $|g\rangle$. In the left panel, $|a\rangle$ is located in a gap between a valence and a conduction band, in the right one it is located within a band—$|a\rangle$ broadens to a resonance of width Δ_a, indicated by the dashing.

the rule for IR photons, irrespective of the nature of the substrate. UV/visible light, on the other hand, couples directly to an adsorbate if an available adsorbate state lies in the energy gap of an insulator or semiconductor surface. If the substrate is a metal, excitation of adsorbates with UV/vis photons is typically indirect (with exceptions), through the substrate. In this case the adsorbate excited state is a *resonance* due to coupling to metal states, rather than a stationary state. The resonance is characterized by a finite electronic lifetime, τ_{el}, related to a resonance width, Δ_a, by

$$\tau_{\mathrm{el}} = \frac{\hbar}{\Delta_a}. \tag{1}$$

For metal surfaces, adsorbate resonance widths can be in the order of 1 eV, and lifetimes as short as femtoseconds. In contrast, adsorbate excited states located within a wide bandgap, energetically well separated from the band edges, have longer lifetimes. The situation is illustrated in figure 1.

Direct and indirect pathways can experimentally be discriminated by a dependence, or lack thereof, of the desorption yield on the polarization of the incoming light. An example for the first class is H:Si(100)2×1, where a strong dependence of the UV-laser induced desorption of hydrogen atoms on the polarization was found [12], in contrast to photodesorption of NO from Pt(111) [13, 14].

The indirect, substrate-mediated excitation can further be categorized according to the fluence dependence of the reaction. With low-fluence, continuous wave (cw) or nanosecond-pulse lasers, one observes so-called *DIET*, desorption induced by electronic transitions, for which the desorption probability Y scales *linearly* with laser fluence. DIET is a result of infrequent, uncorrelated electronic excitations of the adsorbate–substrate complex. For desorption from metals the excited state, often a *negative ion resonance*, is short lived, and desorption occurs in the ground state after quenching. The adsorbate relaxes electronically, within the electronic lifetime τ_{el}, but also vibrationally, on a somewhat longer timescale τ_{vib}. DIET occurs if the average time between two subsequent electronic excitations, t_{exc}, is long as compared to the lifetimes, τ_{el} and τ_{vib}.

In contrast, with intense femtosecond laser (FL) pulses, one observes so-called *DIMET*, desorption induced by multiple electronic transitions. The short laser pulses can cause

more than one, i.e. multiple, excitations of the adsorbate on the timescales of electronic and vibrational relaxation. By the pulse 'hot electrons' are created in the metal surface, which enforce 'ladder climbing' of the adsorbate on the electronic ground state into the desorption continuum.

The FL pulse may also heat surface and bulk phonons, thus leading to thermal desorption. Experimentally, one can discriminate between phonon and electronic mechanisms by *two-pulse correlation* (2PC) traces [15]. Accordingly, one records observables such as the desorption yield Y, as a function of the delay time $\Delta\tau$ between two laser pulses (see below).

For DIMET, pioneered by Heinz and co-workers [15–18], certain 'hallmarks' are the following.

- The desorption yield is usually larger in DIMET than in DIET. It also increases *superlinearly* with laser fluence, F, often according to a power law

$$Y = AF^n \tag{2}$$

  with $n > 1$ (typically 2–10). An example is NO/Pt(111), where at low absorbed fluences up to about 1.5 mJ cm^{-2} $Y \propto F$ is found, and $Y \propto F^{6\pm1}$ at higher fluences [19]. Similar nonlinear scalings (2) were observed in femtosecond laser desorption of NO/Pd(111) [16] (exponent: $n \sim 3.3$), CO/Cu(111) [20] ($n \sim 3.7$), CO/Cu(100) [21] ($n \sim 8$), or O_2/Pd(111) [22, 23] ($n \sim 6$). Nonlinear scaling was also found for photodissociation of O_2 on Pt(111) [24, 25], and photodiffusion of O_2 on Pt(110) [7].
- Besides the desorption yield, other observables may be different under DIMET conditions. For example, the vibrational and translational energy of NO desorbing from Pt(111) both increase with increasing fluence [19].
- Under DIMET or more generally under femtosecond laser (FL) conditions the *branching ratios* of concurring reactions can be different to DIET. For O_2/Pt(111) the preferred reaction is dissociation under ns laser conditions, and desorption when femtosecond lasers are used [24, 25].
- As a result of the nonlinear increase of Y with F, a typical two-pulse correlation signal Y versus $\Delta\tau$ shows a sharp peak around $\Delta\tau = 0$, gradually falling off towards $\Delta\tau \rightarrow \pm\infty$. If the half width at half maximum (HWHM) of $Y(\Delta t)$ is in the ns range, this is indicative for a dominant phononic mechanism, whereas HWHM $\sim$ ps suggests an electronic mechanism instead. The ultrafast response in hot-electron mediated femtosecond laser induced desorption (FLD) is another hallmark of FLD [15].

1.2. Excitation by other energy sources

Similar reactions and processes can be initiated by energy sources other than photons. The best known example is the scanning tunnelling microscope (STM), by which electrons or holes tunnel from an STM tip, thus enforcing nuclear motion. Whether electrons or holes play the part is ruled by the polarity of the sample bias V_s.

An example is STM-induced desorption of H and D atoms from hydrogen-covered Si(100)2 $\times$1 surfaces both at positive and negative sample biases [26–29]. At negative sample bias the lateral 'switching' of a hydrogen atom from one side of a Si_2 dimer to a neighbouring, empty dangling bond site at the same dimer was also observed [30–32]. Apart from this, a number of other processes can be triggered by an STM. Examples are the vibrational excitation of adsorbates by inelastically tunnelling electrons as used in scanning tunnelling spectroscopy, STS [33], the STM-induced diffusion of adsorbates in 'pulling' and 'pushing' modes [34], rotation of molecules [35] or individual units of molecules [36], dissociation [37–39], chemical reactions [40], and STM-induced isomerization [41].

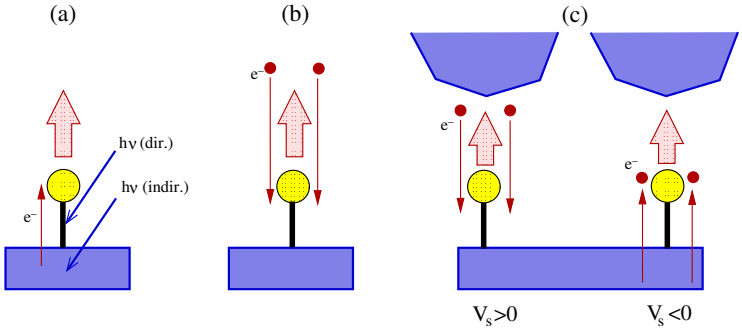

Figure 2. Various electron mediated desorption processes: hot-electron mediated photon stimulated desorption (PSD) (a), ESD (b), and STM induced desorption (c). In (a) also the direct photon excitation, and in (c) two different sample biases V_s are considered. The thick arrows indicate the motion of desorbing adspecies.

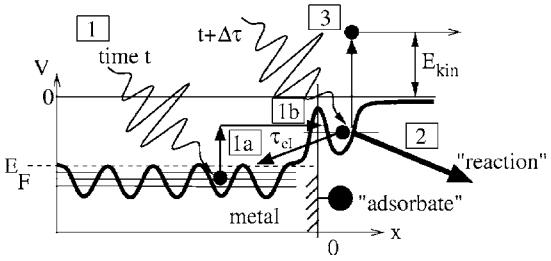

Figure 3. Most important elementary steps of nonadiabatic processes at interfaces. See the text for further explanation.

Similar to photochemistry, different regimes also exist for STM, in which the reaction yield increases either linearly with the tunnelling current I, or in nonlinear fashion. The linear and nonlinear regimes can be realized by choosing the bias voltage above or below a threshold for electronic excitation, respectively. In the 'above threshold' regime, $Y \propto I$, and a single charge carrier emitted from the STM tip provides enough energy to reach the excited state. At semiconductor surfaces this often requires several volts. At lower bias voltages, in the 'below threshold regime', the charge carriers are energetically unable to directly reach the resonance and inelastic electron tunnelling (IET) is the only way to break the bond.

Nonadiabatic surface reactions can also be induced by electrons from other sources. In electron stimulated desorption (ESD), high energy electron beams are used. For example, with 150 keV electrons Menzel and co-workers desorbed CO molecules from a Ru(0001) surface [42, 43]. Various of these 'electron mediated' desorption processes are shown in figure 2.

1.3. Probing nonadiabatic surface dynamics

For laser-induced reactions at interfaces the sketch shown in figure 3 summarizes the most important elementary steps. In the figure, the viewpoint of a single electron is taken, moving in an effective potential along the electron coordinate, x.

The elementary steps indicated are as follows. In step (1), the electron is excited by a laser pulse from a metal Bloch state below the Fermi energy (E_F) into a previously unoccupied level above E_F. The final state can either be a metal state (1a), or a low-lying adsorbate state (1b),

respectively. The transient population of excited intermediates can give rise to various types of 'reactions' (2), such as desorption or dissociation of molecules, or the transport of electrons through molecular junctions. The excitation and de-excitation steps, as well as the reactions involving short-lived excited intermediates, can be probed by time-delayed laser pulses in pump–probe or two-pulse correlation (2PC) modes (3). As a specific example in the figure a two-photon-photoemission (2PPE) experiment is illustrated, where a second pulse emits the electron, which can then be analysed in energy-resolved, time-resolved, and angle-resolved modes respectively. This gives information about the energetic position, the lifetime, and the spatial localization of intermediate states.

1.4. Focus and outline of this review

In this overview we focus on a few recent examples of *nonadiabatic quantum dynamics* induced by photons and electrons, and their spectroscopy. We focus on metal and semiconductor surfaces here, largely ignoring desorption from insulating surfaces, for which the interested reader is referred to the literature [44].

In section 2 we shall present the *models* and *methods* used to describe the nuclear and electron dynamics of these processes. We will also present a few ways of how to compute vibrational and electronic lifetimes, $\tau_{\rm vib}$ and $\tau_{\rm el}$, of adsorbates. In section 3 we shall be concerned with the photodesorption of atoms and molecules from surfaces, emphasizing our own and related work on H/Si(100) and NO/Pt(111).

In section 4 processes and reactions related to photodesorption will be considered. Specific examples are the STM-induced switching and desorption of H at Si(100), the ESD of CO from Ru(0001), and the 2PPE of solvated electrons in ice layers on copper surfaces. Section 5 concludes and summarizes this work.

2. Models and methods for desorption

2.1. Two- and multi-state models

2.1.1. Two-state models. For desorption of adsorbates from insulating surfaces, after direct photoexcitation, one frequently uses two-state models, with a ground state $V_g(R)$, and a single excited state $V_a(R)$. Here, R is a short-hand notation for all nuclear degrees of freedom. In reduced-dimensionality models, only a limited number of 'active' modes is considered, sometimes in fact only one—the 'desorption coordinate', Z, say, typically the distance between the adsorbate and the surface.

The corresponding time-dependent nuclear Schrödinger equation in a *diabatic* representation (see below), is

$$\mathrm{i}\hbar\frac{\partial}{\partial t}\begin{pmatrix}\psi_a\\ \psi_g\end{pmatrix}=\begin{pmatrix}\hat{H}_a & \tilde{V}_{ag}\\ \tilde{V}_{ga} & \hat{H}_g\end{pmatrix}\begin{pmatrix}\psi_a\\ \psi_g\end{pmatrix}. \tag{3}$$

Here, $\psi_n(R)$ is the diabatic nuclear wavefunction on electronic state n, with $n = g, a$. Further,

$$\tilde{V}_{ag}(R,t)=V_{ag}(R)-\left\langle\Psi_a(r,R)\left|\hat{\mu}E(t)\right|\Psi_g(r,R)\right\rangle_r \tag{4}$$

is an electronic coupling matrix element connecting states $|g\rangle$ and $|a\rangle$. The second term in equation (4) is a direct field coupling, written here in the semiclassical dipole approximation, with $E(t)$ being the electric field, and

$$\left\langle\Psi_a(r,R)\left|\hat{\mu}\right|\Psi_g(r,R)\right\rangle_r:=\mu_{ag}(R) \tag{5}$$

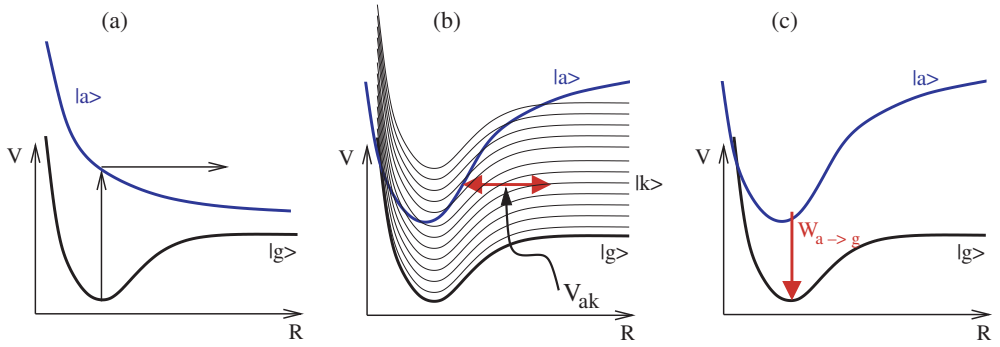

Figure 4. (a) Illustration of the coupled two-state model, typically realized for insulating surfaces. The ground state $|g\rangle$ and a photoactive excited state $|a\rangle$ are indicated. (b) The coupled multi-state model, typically realized for photochemistry at metal surfaces, with ground state $|g\rangle$, a photoactive excited state $|a\rangle$, and a continuum of states $|k\rangle$. A specific coupling element V_{ak} is indicated by the double arrow. (c) Illustration of an effective two-state model, with transition rate $W^{\mathrm{el}}_{a\to g} = \Delta_a/\hbar$.

the transition dipole moment, which can be calculated from the electronic wavefunctions $\Psi_g(r, R)$ and $\Psi_a(r, R)$, and the dipole operator $\hat{\mu}$. The letter r is a short-hand notation for all electronic coordinates; the vector character of the field and the transition dipole moment has also been omitted for convenience. The first term in equation (4) is a nonadiabatic coupling function $V_{ag}(R)$. The latter accounts for radiationless transitions due to non-Born–Oppenheimer or spin-orbit effects, again expressed in diabatic representation. The radiationless couplings are often neglected in two-state models. Note that the diagonal elements $\tilde{V}_{nn}$ were also neglected here, i.e.

$$\hat{H}_n = \hat{T}_R + V_n(R) \tag{6}$$

where $\hat{T}_R$ is the nuclear kinetic energy operator.

Equation (3) holds for the situation shown in figure 1(a), i.e. direct excitation of an adsorbate state $|a\rangle$ located within a large bandgap. The final state has an infinite lifetime on the timescale of the reaction, $\tau_{\mathrm{el}} \to \infty$, and the vibrational lifetime due to coupling of adsorbate modes to substrate phonons (and electron–hole pairs) was assumed to be finite. As a consequence, the total energy is conserved in this model, and desorption, if it happens, takes place in the excited state. The situation we have in mind is illustrated in figure 4(a).

2.1.2. Multi-state models. When the situation in figure 1(b) is considered instead, which pertains to metal surfaces, the inclusion of continuum states is required. The coupling of an excited, photoactive adsorbate state, $|a\rangle$, to substrate continuum states, $|k\rangle$, can be modelled by generalizing equation (3) as

$$\mathrm{i}\hbar\frac{\partial}{\partial t}\begin{pmatrix}\psi_a\\ \psi_g\\ \psi_{k_1}\\ \psi_{k_2}\\ \vdots\end{pmatrix} = \begin{pmatrix}\hat{H}_a & \tilde{V}_{ag} & \tilde{V}_{ak_1} & \tilde{V}_{ak_2} & & \cdots\\ \tilde{V}_{ga} & \hat{H}_g & \tilde{V}_{gk_1} & \tilde{V}_{gk_2} & & \cdots\\ \tilde{V}_{k_1a} & \tilde{V}_{k_1g} & \hat{H}_{k_1} & \tilde{V}_{k_1k_2} & \tilde{V}_{k_1k_3} & \cdots\\ \tilde{V}_{k_2a} & \tilde{V}_{k_2g} & \tilde{V}_{k_2k_1} & \hat{H}_{k_2} & \tilde{V}_{k_2k_1} & \cdots\\ \vdots & \vdots & \vdots & \vdots & \vdots & \ddots\end{pmatrix}\begin{pmatrix}\psi_a\\ \psi_g\\ \psi_{k_1}\\ \psi_{k_2}\\ \vdots\end{pmatrix}. \tag{7}$$

Here, $\psi_n(R)$ is the nuclear wavefunction on state $|n\rangle$. Also in this model the energy is conserved. The non-diagonal elements $\tilde{V}_{nm}(t)$ account for non-Born–Oppenheimer and optical

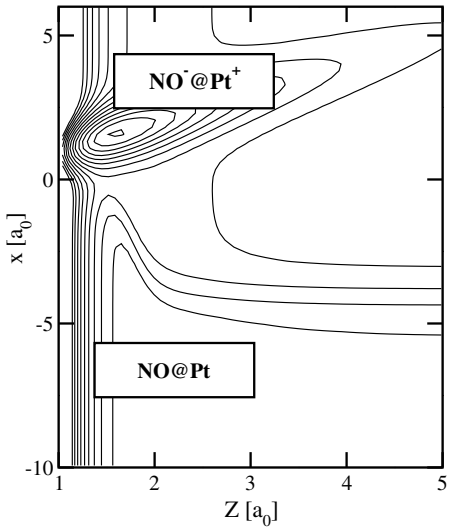

Figure 5. Model potential $V(x, Z)$ for NO in front of a Pt(111) film, 30 a_0 thick, shown as a contour plot. A modified version of the potential of [50] was used, with details given in [51]. The electron coordinate is x, where $x > 0$ corresponds to an electron outside the surface; the NO–surface distance is Z. A wavepacket localized in the well in front of the surface corresponds to an NO^- ion, while the area with $x < 0$ corresponds to neutral NO.

couplings in general again. We have again assumed that only a single resonance state $|a\rangle$ exists. The non-Born–Oppenheimer coupling between $|a\rangle$ and the metal continuum states $|k\rangle$ is accomplished by coupling functions $V_{ak}(R)$, similar to those appearing in the Newns–Anderson model [45–47]. The situation we have in mind is illustrated in figure 4(b).

Substrate mediated excitation of $|a\rangle$ is described in this model by direct optical excitation of metal states $|k\rangle$, and subsequent coupling to adsorbate state $|a\rangle$. Desorption occurs in either $|g\rangle$ or one of the metal excited states $|k\rangle$, after rapid depopulation of $|a\rangle$. The $|a\rangle$ state is nevertheless essential, because it sets the wavepacket in motion. In figure 4(b), $V_a(R)$ is bound and shifted towards the surface ($R = Z$), which is typical for an image charge stabilized negative ion resonance. This is called an Antoniewicz scenario [48]. Other potential forms for $V_a(Z)$, such as the purely repulsive potential shown in figure 4(a), will also lead to desorption—this is the well known Menzel–Gomer–Redhead (MGR) model [49].

2.2. Nuclear–electron wavepacket methods

A related approach was introduced some time ago by Holloway and co-workers [50]. Their model is based on coupled electron–nuclear wavepacket propagation. Accordingly, one solves a time-dependent Schrödinger equation

$$\mathrm{i}\hbar \frac{\partial \Psi_{\mathrm{tot}}(r, R, t)}{\partial t} = \left(\hat{T}_R + \hat{T}_r + V(r, R)\right) \Psi_{\mathrm{tot}}(r, R, t) \tag{8}$$

for the *total*, electron–nuclear wavefunction $\Psi_{\mathrm{tot}}(r, R, t)$. $\hat{T}_r$ and $\hat{T}_R$ are kinetic energy operators for electrons and nuclei, and $V(r, R) = V_{rr} + V_{rR} + V_{RR}$ contains all potential terms, i.e. electron–electron repulsion, electron–nuclear attraction, and internuclear repulsion. In [50] the model was applied to the photodesorption of NO from Pt, with one electronic ($r = x$) and one nuclear ($R = Z$) degree of freedom. $V(x, Z)$ was chosen as a suitable model potential, which is shown in figure 5. Note that a one-dimensional cut of $V(x, Z)$ along the electron

coordinate x, at a fixed value of Z, corresponds to the situation shown in figure 3, with an adsorbate well separated by a barrier from the bulk.

As initial states, $\Psi_{\rm tot}(x, Z, 0) = g(x)\,\phi_n(Z)$ products made of a Gaussian electronic wavepacket moving towards the surface and a bound NO vibrational state $\phi_n(Z)$ were taken in [50]. Solution of equation (8) and collecting the wavefunction at large Z then gives the desorption probability, with all non-Born–Oppenheimer couplings accounted for.

Apart from the fact that it is not clear how to construct $V(x, Z)$, the method is also numerically costly since the light electron and the heavy nucleus have to be propagated simultaneously on a grid. Further, the laser-excitation step was neglected. Some of these drawbacks can be overcome by expanding the total wavefunction as

$$\Psi_{\rm tot}(r, R, t) = \sum_n \Psi_n(r, R)\psi_n(R, t). \tag{9}$$

Here, the Ψ_n are again the electronic wavefunctions depending parametrically on R, and $\psi_n(R, t)$ is the nuclear wavefunction on state $|n\rangle$. There are various ways to choose the electronic basis functions $\Psi_n(r, R)$. In an *adiabatic* representation, $\Psi_n = \Psi_n^{\rm a}$ ('a' = adiabatic), is evaluated from the eigenvalue equation

$$\left(\hat{T}_r + V(r, R)\right)\Psi_n^{\rm a}(r, R) = V_n^{\rm a}(R)\Psi_n^{\rm a}(r, R) \tag{10}$$

for each parameter value R. This results in a coupled time-dependent Schrödinger equation for the nuclei, which we write in the form

$$\mathrm{i}\hbar\frac{\partial\psi_n^{\rm a}(r, t)}{\partial t} = \sum_m \left(\hat{K}_{nm}^{\rm a} + V_{nm}^{\rm a} - \mu_{nm}^{\rm a}E(t)\right)\psi_m^{\rm a}(r, t). \tag{11}$$

Equation (11) is the adiabatic analogue of the matrix equation (7). Note that now we also include the diagonal terms $\hat{K}_{mm}^{\rm a}$ and $\mu_{mm}^{\rm a}E(t)$ for completeness. The adiabatic potential matrix $\underline{\underline{V}}^{\rm a}$ is diagonal with elements $V_{nm}^{\rm a}(R) = \langle\Psi_n^{\rm a}|V(r, R)|\Psi_m^{\rm a}\rangle_r = \delta_{nm}V_n^{\rm a}(R)$, where $V_n^{\rm a}$ are adiabatic potential curves. The kinetic coupling matrix elements $\hat{K}_{nm}^{\rm a}$ contain the well known first and second order derivative couplings, in a one-dimensional model ($R = Z$), given by

$$\hat{K}_{nm}^{\rm a} = -\frac{\hbar^2}{2m}\left[\left\langle\Psi_n^{\rm a}\left|\frac{\mathrm{d}^2\Psi_m^{\rm a}}{\mathrm{d}Z^2}\right.\right\rangle + 2\left\langle\Psi_n^{\rm a}\left|\frac{\mathrm{d}\Psi_m^{\rm a}}{\mathrm{d}Z}\right.\right\rangle\frac{\mathrm{d}}{\mathrm{d}Z}\right], \tag{12}$$

where m is the mass for motion along Z. In equation (11) dipole coupling to an external field is included through dipole matrix elements $\mu_{nm}^{\rm a} = \langle\Psi_n^{\rm a}|\hat{\mu}(r, R)|\Psi_m^{\rm a}\rangle_r$, now in adiabatic representation.

Adiabatic electronic wavefunctions could be obtained from quantum chemistry programs which start from the Born–Oppenheimer approximation. By a configuration interaction type calculation, for example, using cluster models, one obtains ground and excited state wavefunctions $\Psi_g^{\rm a}$, $\Psi_a^{\rm a}$, and $\Psi_k^{\rm a}$. From these, the derivative couplings $\frac{\mathrm{d}\Psi_m^{\rm a}}{\mathrm{d}Z}$ and $\frac{\mathrm{d}^2\Psi_m^{\rm a}}{\mathrm{d}Z^2}$ and the dipole coupling matrix elements $\mu_{mn}^{\rm a}$ can be obtained. This represents, therefore, a route by which the coupled nuclear–electron wavepacket model could be realized *ab initio* [52]. Large-scale CI and multi-reference CI calculations have recently been carried out for systems such as N_2/Pt_{64} [53], CO/Pt_{97}, and H_2CO/Ag_{97} [54, 55]. It must be noted, however, that in these calculations metal excitations were not considered, and no dipole or derivative couplings were determined. Other serious problems are that the number of excited states increases rapidly with cluster size, and that properties converge notoriously slowly with increasing cluster size [56, 57]. It is still possible that the cluster ansatz can be used, perhaps with alternative methods such as time-dependent density functional theory [58–60], to treat DIET and DIMET from metals from first principles. Until then, model potentials such as $V(x, Z)$ as suggested by Holloway and co-workers are useful.

For practical purposes the adiabatic representation is not optimal. The couplings $\hat{K}^{\mathrm{a}}_{mn}$ are momentum-dependent operators, which peak sharply around 'avoided' crossings (and more generally around conical intersections) of adiabatic potential energy curves (and surfaces). A representation which avoids singularities is the *diabatic* representation. Here, a reference geometry R_0 for the nuclei is chosen, and the eigenvalue equation

$$\left(\hat{T}_r + V(r;\, R_0)\right) \Psi_n(r;\, R_0) = V_n(R_0)\Psi_n(r;\, R_0) \tag{13}$$

solved. This results in a coupled time-dependent Schrödinger equation for the nuclei in diabatic representation (for which we use no superscript)

$$\mathrm{i}\hbar \frac{\partial \psi_n(r,t)}{\partial t} = \sum_m \left(\hat{K}_{nm} + V_{nm} - \mu_{nm} E(t)\right) \psi_m(r,t). \tag{14}$$

Now, the potential matrix with elements $V_{nm} = \langle \Psi_n | V(r, R) | \psi_m \rangle_r$ is full, while $\hat{K}_{nm} = \hat{T}_R \delta_{nm}$ is diagonal. Further, the dipole matrix is different in the diabatic representation from the adiabatic one. Different choices of the reference geometry R_0 constitute different diabatic representations. Once adiabatic potential energy surfaces and wavefunctions have been calculated *ab initio*, it is straightforward to transform to the diabatic picture if in addition the kinetic coupling operators are known [52, 61, 62]. It should be mentioned that the diabatization scheme above with a specific choice R_0 is only one of many other, more sophisticated schemes which were suggested in the literature. The reader is referred to [63] for a comprehensive overview.

The diabatic Schrödinger equation (14) is equivalent to the multi-state model of equation (7), where, however, the diagonal terms have been neglected. It is also equivalent to equation (8), from which it was derived. However, neither equation (7) nor equations (11) or (14) can be solved efficiently because too many metal states $|k\rangle$ would be needed to converge the expansion equation (9). To improve on this, in [51] a special diabatic representation has been suggested, called the 'extended close coupling' (ECC) scheme. In this scheme diabatic states are generated not from a single reference point R_0, but from a set of various reference points $\{R_{0i}\}$ instead, and orthogonalized to each other. In this way, with a smaller number of diabatic surfaces converged results can be obtained. As a result it was possible, within the potential model of Holloway, to treat photodesorption of NO from rather thick metal films representing a Pt surface, as shown below.

Again it must be noted, though, that the analytic expression of the Holloway potential $V(x, Z)$ and its parameters are 'arbitrary' in their present form, or semiempirical at best, with no firm *ab initio* basis. Quantitative statements cannot be expected, therefore, from this model.

2.3. Open-system density matrix theory

2.3.1. DIET. An alternative to energy-conserving multi-state models is open-system density matrix theory within an effective, dissipative two-state model. Quite generally in this theory one solves instead of a Schrödinger equation for a closed system an open-system Liouville–von Neumann equation

$$\frac{\partial \hat{\rho}}{\partial t} = \mathcal{L}\hat{\rho} + \mathcal{L}_{\mathrm{D}}\hat{\rho}. \tag{15}$$

Here, $\hat{\rho}$ is the density operator of a (small sub-) system, which evolves under the influence of a (Hamiltonian) Liouvillian $\mathcal{L} = -\frac{\mathrm{i}}{\hbar}[\hat{H}_{\mathrm{s}}, \hat{\rho}]$, with $\hat{H}_{\mathrm{s}}$ being the system Hamiltonian, which may contain direct system–field coupling. Further, $\mathcal{L}_{\mathrm{D}}$ is the dissipative Liouvillian which accounts for the coupling to an environment. In equation (15) the so-called Markov approximation has

been made, i.e. $\frac{\partial\hat{\rho}}{\partial t}$ depends on $\hat{\rho}(t)$ only. Lindblad showed that in order to have a strictly positive time evolution of the density operator a dissipative, Markovian Liouvillian must obey the form [64–66]

$$\mathcal{L}_{\mathrm{D}}\hat{\rho} = \sum_n \left(\hat{C}_n\hat{\rho}\hat{C}_n^\dagger - \tfrac{1}{2}\left[\hat{C}_n^\dagger\hat{C}_n, \hat{\rho}\right]_+\right). \tag{16}$$

Here, $[,]_+$ denotes an anticommutator, n labels various dissipation channels (e.g. energy relaxation, pure dephasing), and $\hat{C}_n$ is a Lindblad operator specifying the nature and strength of this channel.

Within the dissipative two-state model of DIET, the Liouville–von Neumann (LvN) equation is [67, 68]

$$\frac{\partial}{\partial t}\begin{pmatrix}\hat{\rho}_a & \hat{\rho}_{ag}\\ \hat{\rho}_{ga} & \hat{\rho}_g\end{pmatrix} = -\frac{\mathrm{i}}{\hbar}\left[\begin{pmatrix}\hat{H}_a & \tilde{V}_{ag}\\ \tilde{V}_{ga} & \hat{H}_g\end{pmatrix}\begin{pmatrix}\hat{\rho}_a & \hat{\rho}_{ag}\\ \hat{\rho}_{ga} & \hat{\rho}_g\end{pmatrix}\right] + \frac{\partial}{\partial t}\begin{pmatrix}\hat{\rho}_a & \hat{\rho}_{ag}\\ \hat{\rho}_{ga} & \hat{\rho}_g\end{pmatrix}_{\mathrm{D}}. \tag{17}$$

In equation (17) the $\hat{\rho}_i$ and $\hat{\rho}_{ij}$ are operators in the vibrational space of the ground and excited state vibrational functions $\{|\phi_\alpha^g\rangle\}$ and $\{|\phi_\alpha^{\mathrm{a}}\rangle\}$. The last term in equation (17), in somewhat sloppy notation, accounts generally for energy and phase relaxation, but also for substrate-mediated excitation. Within the Lindblad approach, energy relaxation of the excited state $|a\rangle$ of width Δ_a with a rate

$$W_{a\to g}^{\mathrm{el}} = \frac{\Delta_a}{\hbar} \tag{18}$$

gives rise to

$$\frac{\partial}{\partial t}\begin{pmatrix}\hat{\rho}_a & \hat{\rho}_{ag}\\ \hat{\rho}_{ga} & \hat{\rho}_g\end{pmatrix}_{\mathrm{D},1} = -W_{a\to g}^{\mathrm{el}}\begin{pmatrix}\hat{\rho}_a & \frac{\hat{\rho}_{ag}}{2}\\ \frac{\hat{\rho}_{ga}}{2} & -\hat{\rho}_a\end{pmatrix}. \tag{19}$$

DIET is modelled by a single Franck–Condon excitation of the ground state wavefunction ϕ_0^g to the excited state, i.e. $\hat{\rho}_0 = |a\rangle\langle a| \otimes |\phi_0^g\rangle\langle\phi_0^g|$. Further, equation (19) is then the only 'dissipative' term entering equation (17). This corresponds to an electronic Liouvillian $\mathcal{L}_{\mathrm{D}}^{\mathrm{el}}$ with a single Lindblad operator

$$\hat{C}_1^{\mathrm{el}} = \sqrt{W_{a\to g}^{\mathrm{el}}}|g\rangle\langle a|. \tag{20}$$

The resonance width Δ_a (and the rate $W_{a\to g}^{\mathrm{el}}$) depends in general on R. If this dependence is neglected, the resonance decays strictly exponentially with the lifetime $\tau_{\mathrm{el}} = \frac{1}{W_{a\to g}^{\mathrm{el}}}$. The effective two-state model with a decaying upper electronic state, as an alternative to a non-dissipative multi-state model, is illustrated in figure 4(c).

In addition, *vibrational relaxation* can be included via a total Liouvillian $\mathcal{L}_{\mathrm{D}}^{\mathrm{vib}} + \mathcal{L}_{\mathrm{D}}^{\mathrm{el}}$. For the dissipative, vibrational Liouvillian $\mathcal{L}_{\mathrm{D}}^{\mathrm{vib}}$, one may also use a Lindblad form. If vibrational relaxation is only considered for the ground state, we have

$$\left(\frac{\mathrm{d}\rho_{g,\alpha\alpha}}{\mathrm{d}t}\right)_{\mathrm{D}}^{\mathrm{vib}} = \sum_\beta W_{\beta\to\alpha}^{\mathrm{vib}}\rho_{g,\beta\beta} - \sum_\beta W_{\alpha\to\beta}^{\mathrm{vib}}\rho_{g,\alpha\alpha} \tag{21}$$

for the diagonal elements of the ground state density matrix, and

$$\left(\frac{\mathrm{d}\rho_{g,\alpha\beta}}{\mathrm{d}t}\right)_{\mathrm{D}}^{\mathrm{vib}} = -\gamma_{\alpha\beta}\rho_{g,\alpha\beta} \tag{22}$$

for the off-diagonal elements of $\hat{\rho}_g$, i.e. $\rho_{g,\alpha\beta} = \langle\phi_\alpha^g|\hat{\rho}_g|\phi_\beta^g\rangle$. Here, the $W_{\alpha\to\beta}^{\mathrm{vib}}$ are environment induced transition rates connecting vibrational levels $|\alpha\rangle = |\phi_\alpha^g\rangle$ and $|\beta\rangle$. The rates obey detailed balance,

$$W_{\alpha\to\beta}^{\mathrm{vib}} = W_{\beta\to\alpha}^{\mathrm{vib}}\exp\left\{-\frac{E_\beta - E_\alpha}{k_{\mathrm{B}}T_{\mathrm{ads}}}\right\} \tag{23}$$

where $T_{\rm ads}$ is the temperature (if any exists) for the adsorbate vibration under consideration. The two major mechanisms for vibrational relaxation are vibration–phonon coupling and vibration–electron coupling, as outlined in greater detail below.

The above formalism can also be extended to unbound ground state potentials, and be expressed in configuration space rather than eigenstate representation. One route to do so is to use approximate raising and lowering operators [69–71] similar to those used in so-called supersymmetric quantum mechanics (SUSY QM) [72]. However, other dissipative Liouvillians have also been suggested which achieve the same goal [73–75].

2.3.2. DIMET. When intense femtosecond lasers are used for photodesorption, DIMET is possible. In the two-state density matrix model the hot-electron, substrate mediated excitation can be modelled by an extra term in equation (17) [67, 68]:

$$\frac{\partial}{\partial t}\begin{pmatrix}\hat{\rho}_a & \hat{\rho}_{ag}\\ \hat{\rho}_{ga} & \hat{\rho}_g\end{pmatrix}_{\rm D,2} = W^{\rm el}_{g\to a}(t)\begin{pmatrix}\hat{\rho}_g & -\frac{\hat{\rho}_{ag}}{2}\\ -\frac{\hat{\rho}_{ga}}{2} & -\hat{\rho}_g\end{pmatrix}. \tag{24}$$

In DIMET, the initial condition is $\hat{\rho}_0 = |g\rangle\langle g| \otimes |\phi^g_0\rangle\langle\phi^g_0|$ if $T = 0$ initially. Further,

$$W^{\rm el}_{g\to a}(t) = W^{\rm el}_{a\to g}\exp\left\{-\frac{V_a - V_g}{k_{\rm B}T_{\rm el}(t)}\right\} \tag{25}$$

is a time-dependent upward rate that obeys detailed balance. Equation (24) corresponds to a Lindblad operator

$$\hat{C}^{\rm el}_2 = \sqrt{W^{\rm el}_{g\to a}(t)}|a\rangle\langle g|. \tag{26}$$

Direct excitation can enter the Hamiltonian matrix $\underline{\underline{H}}$ through dipole-coupling terms. Again, vibrational relaxation can be included as outlined above [71].

When calculating the upward rate in equation (25) we assumed that hot electrons have been created by the laser pulse, characterized by an electronic temperature $T_{\rm el}(t)$. The latter can be estimated from the well known two-temperature (2TM) model [76–78]. Accordingly, one solves two coupled equations

$$C_{\rm el}\frac{\partial T_{\rm el}}{\partial t} = \frac{\partial}{\partial x}K\frac{\partial}{\partial x}T_{\rm el} - g(T_{\rm el} - T_{\rm ph}) + S(x,t) \tag{27}$$

$$C_{\rm ph}\frac{\partial T_{\rm ph}}{\partial t} = g(T_{\rm el} - T_{\rm ph}) \tag{28}$$

for the electron and phonon temperatures $T_{\rm el}$ and $T_{\rm ph}$, at a position x relative to the surface. In equation (27), $C_{\rm el}$ and $C_{\rm ph}$ are the electron and lattice specific heat constants. According to equation (27) the electron temperature changes due to thermal diffusion (first term on the right, with K = thermal conductivity of the electrons), electron–phonon coupling (second term, with g = electron–phonon-coupling constant), and the external laser pulse (third term). The source term can be calculated, for a metal film of thickness L, as [78]

$$S(x,t) = \frac{AI(t)\exp(-\alpha x)}{1 - \exp(-\alpha L)}. \tag{29}$$

Here $AI(t)$ is the absorbed fraction of the intensity I of a laser pulse and α^{-1} is the optical penetration depth.

As an example we show in figure 6(a) the phonon and electron temperatures at a Pt surface ($L \to \infty$), after a Gaussian laser pulse with FWHM 80 fs was applied. The electron temperature rises on a sub-ps timescale to a maximal value $T^{\rm max}_{\rm el}$ of a few thousand K, while the phonon temperature never reaches temperatures this high. It is also found that the maximal electronic temperature increases in good approximation with the laser fluence, F, according to $T^{\rm max}_{\rm el} \propto \sqrt{F}$. This is indicated in figure 6(b), and supported by earlier theoretical [79] and experimental [78] evidence.

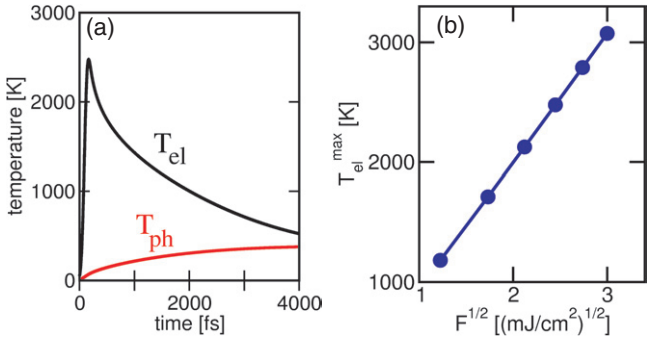

Figure 6. (a) $T_{\rm el}(t)$ and $T_{\rm ph}$ curves according to the two-temperature model, for a Pt surface when a Gaussian pulse of width FWHM = 80 fs, fluence $F = 6$ mJ cm^{-2}, and wavelength $\lambda = 619$ nm was applied, at $t = 0$. The initial temperature was 85 K [71]. (b) Dependence of the maximal electronic temperature $T_{\rm el}^{\rm max}$ on the laser fluence, F.

2.3.3. Numerical solution of LvN equations. The Liouville–von Neumann equations can be solved by direct propagation of density matrices on a grid, or in (system) eigenstate representation. This can be costly and is therefore limited to one or two system degrees of freedom when 'standard methods' are used [80–82]. A way out is stochastic wavepacket methods, such as the Monte Carlo wavepacket (MCWP) scheme [83–86], by which the LvN equation can be unravelled exactly, in the limit $M \to \infty$, by propagating a set of M 'quantum trajectories' $\psi_n(t), n = 1, \ldots, M$, the latter selected by a stochastic process.

A special and very efficient variant of this theory was introduced by Gadzuk within his 'jumping wavepacket' model [87, 88]. Here, the DIET (at $T = 0$) is treated in two steps. In step one, the ground state wavefunction ϕ_0^g is projected on the excited state $|a\rangle$, propagated there for a reference time $\tau_{\rm R}$, damped to the ground state $|g\rangle$, and propagated to a time of interest, t:

$$|\psi(t;\tau_{\rm R})\rangle = \exp\left\{-\frac{{\rm i}\hat{H}_g(t-\tau_{\rm R})}{\hbar}\right\}|g\rangle\langle a|\exp\left\{-\frac{{\rm i}\hat{H}_a\tau_{\rm R}}{\hbar}\right\}|\phi_0^g\rangle. \tag{30}$$

To compute observables, in the second step an incoherent averaging scheme is adopted. Assuming a coordinate-independent resonance width $\Delta_a = \hbar/\tau_{\rm el}$, the excited state decays exponentially and observables are given by

$$\left\langle\hat{A}\right\rangle(t) = \frac{1}{\tau_{\rm el}}\int_0^\infty {\rm e}^{-\tau_{\rm R}/\tau_{\rm el}}\left\langle\psi(t;\tau_{\rm R})|\hat{A}|\psi(t;\tau_{\rm R})\right\rangle {\rm d}\tau_{\rm R}. \tag{31}$$

In practice, (31) is evaluated as a sum over M' residence times τ_{R_i}, chosen from an appropriate interval. For coordinate-independent quenching, Gadzuk's algorithm is equivalent to the open-system density matrix approach, as it turns out to be a special variant of the MCWP method [89–91]. This is useful, because the jumping wavepacket method requires fewer quantum trajectories in comparison to the ordinary MCWP scheme, i.e. $M' \ll M$. The MCWP or related methods are more general, however, and can also be applied for DIMET, as demonstrated in [89, 91, 92].

2.4. Electronic friction models

The substrate-mediated laser desorption from metal surfaces is frequently modelled as 'ladder climbing' in the electronic ground state up to the desorption continuum. The starting point

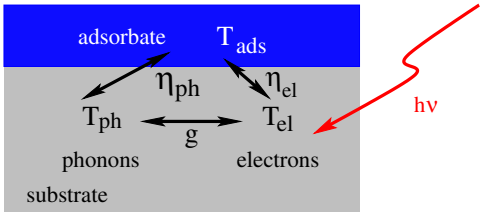

Figure 7. Illustration of two- and three-temperature models. An initial laser pulse heats the metal electrons, which are directly or indirectly coupled to substrate phonons and the adsorbate vibrations.

is two- or three-temperature models, associated with two or three 'reservoirs', i.e. electrons, phonons, and the adsorbate, as illustrated in figure 7. The subsystems are coupled by characteristic coupling constants. Metal electrons to phonons by the electron–phonon coupling constant g, metal electrons to the adsorbate by a vibration–electron constant η_{el}, and phonons to the adsorbate by a vibration–phonon coupling constant η_{ph}.

In a typical FLD experiment the laser pulse heats the electrons to a time-dependent temperature, $T_{\mathrm{el}}(t)$. Through electron–phonon coupling phonons are also heated, giving rise to a phonon temperature $T_{\mathrm{ph}}(t)$. Without an adsorbate, this is the two-temperature model as described above. The adsorbate–surface bond can be heated to an adsorbate temperature, $T_{\mathrm{ads}}(t)$, either by the electrons through the coupling constant η_{el}, or by the phonons through η_{ph}.

If the electronic channel dominates, which is often the case, it was shown in [93] from a Langevin model for the electron heat bath that, after various simplifications, a classical differential equation is obtained for the adsorbate temperature:

$$\frac{\partial T_{\mathrm{ads}}}{\partial t} = \eta_{\mathrm{el}}\,(T_{\mathrm{el}} - T_{\mathrm{ads}})\,. \tag{32}$$

Equation (32) has to be solved in addition to the 2TM equations (27) and (28), leading to the three-temperature model (3TM). In the classical limit [93], the desorption rate is then given as

$$R_{\mathrm{des}} = \frac{\mathrm{d}Y(t)}{\mathrm{d}t} = \frac{D\eta_{\mathrm{el}}}{k_{\mathrm{B}}T_{\mathrm{ads}}(t)} \exp\left\{-\frac{D}{k_{\mathrm{B}}T_{\mathrm{ads}}(t)}\right\}. \tag{33}$$

The quantities D and η_{el} are often used as model parameters to fit experimental data, and can be interpreted as an effective activation energy, and the rate for energy transfer from the adsorbate to the surface by vibration–electron coupling, respectively.

The Arrhenius model above, and similar ones [15, 18, 22], allow for a beautiful physical interpretation and analysis but are inherently classical and 'one dimensional'. Apart from this, the concept of an electron temperature is questionable at least within the first few hundred femtoseconds after the pulse according to experimental [94] and theoretical investigation [95, 96]. Also, the validity of an adsorbate temperature is disputable [71, 97].

Some of the above restrictions can be overcome by molecular dynamics which includes electronic friction. This approach was popularized by Tully and co-workers [98]. In their method the nuclear motion is classical, and the electronic degrees of freedom are expressed in the form of friction and fluctuating forces. If q is the only degree of freedom considered (e.g. , the molecule–surface distance Z, mass m_q), the equation of motion is

$$m_q \frac{\mathrm{d}^2 q}{\mathrm{d}t^2} = -\frac{\mathrm{d}V}{\mathrm{d}q} - \eta_{qq}\frac{\mathrm{d}q}{\mathrm{d}t} + R_q(t). \tag{34}$$

Here, V is the ground state potential, and η_{qq} is related to the electronic friction coefficient above through $\eta_{qq} = m_q \eta_{\mathrm{el}}$. $R_q(t)$ is a fluctuating force that obeys a fluctuation–dissipation theorem,

$$\left\langle R_q(t) | R_q(t') \right\rangle = 2k_{\mathrm{B}} T_{\mathrm{el}} \eta_{qq} \delta(t - t'), \tag{35}$$

and depends on the electronic temperature. Equation (34) can be easily generalized to more than one degree of freedom, by interpreting the friction coefficient as a tensor with elements $\eta_{qq'}$ [98, 99]. This approach has been used for FLD for CO from Cu surfaces, by Head-Gordon and co-workers [100, 101]. In this case the electronic temperature in equation (35) is large and time dependent, according to the 2TM, and hence the fluctuating forces are large. A molecule, kicked by the random forces, can overcome the binding energy, D, and desorb.

Finally, the classical approximation can be overcome with the help of master equations, derived from open-system density matrix theory. For example, in [102] it was shown, starting from a model Hamiltonian of the Newns–Anderson type, that a master equation

$$\frac{\mathrm{d}P_\alpha}{\mathrm{d}t} = \sum_\beta W_{\beta\to\alpha} P_\beta(t) - \sum_\beta W_{\alpha\to\beta} P_\alpha(t) \tag{36}$$

emerges for the population $P_\alpha = \rho_{g,\alpha\alpha}$ of state $|\alpha\rangle$ of the ground state potential. The hot-electron driven transition rates, calculated from perturbation theory, are functions of the electron temperature $T_{\mathrm{el}}(t)$, and of the energetic position ε_a and width Δ_a of the adsorbate resonance responsible for desorption [97, 102, 103]. By solving equation (36), the desorption probability can be defined as

$$Y(t) = 1 - \sum_{\alpha \in N_{\mathrm{b}}} P_\alpha(t) \tag{37}$$

where N_{b} is the number of bound states, with an energy $E_\alpha \leqslant D$, and D is the binding energy of the adsorbate. In certain limits, in particular in the so-called 'truncated harmonic oscillator' (THO) model, and when it is assumed that the P_α follow a Boltzmann distribution corresponding to a vibrational temperature T_{ads}, the master equation (36) can further be simplified, resulting in a desorption rate R_{des} of the Arrhenius type (33) [155].

2.5. Energy transfer to the substrate

The knowledge of the vibrational and electronic lifetimes τ_{vib} and τ_{el} of adsorbates, by energy transfer to the surface, is central to many theories of photodesorption.

2.5.1. Vibrational relaxation. The vibrational damping coefficient η and vibrational lifetime, τ_{vib}, of an adsorbate vibration is defined, for finite temperatures, as [104]

$$\eta = W_{1\to 0} - W_{0\to 1} = \tau_{\mathrm{vib}}^{-1}. \tag{38}$$

The two most important mechanisms for vibrational energy relaxation at surfaces are vibration–phonon and vibration–electron coupling, both with individual contributions to η:

$$\eta = \eta_{\mathrm{ph}} + \eta_{\mathrm{el}} = {\tau_{\mathrm{vib}}^{\mathrm{ph}}}^{-1} + {\tau_{\mathrm{vib}}^{\mathrm{el}}}^{-1}. \tag{39}$$

Vibrational lifetimes were measured for a variety of systems. An interesting case is the internal stretch mode of adsorbed CO, where vibrational lifetimes of ∼4.3 ms, ∼2.3 ns, and ∼3 ps were reported for NaCl(100) [105], Si(100) [106], and Cu(100) [107] surfaces. Both for the insulator and the semiconductor, relaxation by vibration–electron hole pair coupling is inefficient, because the fundamental energy gap between valence and conduction band is much larger than the vibrational quantum $\hbar\omega_0$ of about 2100 cm^{-1}. Since this frequency is also much

higher than the Debye frequency of a typical substrate of a few hundred cm^{-1} [108], direct energy transfer to substrate phonons is also slow. As a consequence, the vibrational lifetime is long. Long lifetimes are also characteristic for other high-frequency adsorbate modes on nonmetallic surfaces, such as the Si–H stretch vibration of H:Si(100)2 × 1 [109] (see below). For CO/Cu(100), the phononic decay channel is also inefficient. The short lifetime in the ps range is the result of the coupling of the CO stretch mode to electron–hole pairs of the metal [98, 110, 111].

Both the vibration–phonon and the vibration–electron coupling, are frequently calculated perturbatively. For this purpose, the total Hamiltonian is written as

$$\hat{H}_{\mathrm{tot}} = \hat{H}_{\mathrm{s}} + \hat{H}_{\mathrm{b}} + \hat{H}_{\mathrm{sb}}. \tag{40}$$

Here, $\hat{H}_{\mathrm{s}}$ is the system Hamiltonian which supports the vibrational states $|\alpha\rangle$ of the adsorbate–substrate complex. $\hat{H}_{\mathrm{b}}$ is the 'bath' Hamiltonian which supports the bath states $|k\rangle$, and $\hat{H}_{\mathrm{sb}}$ is the coupling between the two. Considering again a single adsorbate vibration, q, according to Fermi's golden rule the transition rate between $v = 1$ and 0 of the adsorbate vibration is

$$W_{1\to 0} = \frac{2\pi}{\hbar} \sum_i \sum_f w_i(T)(1 - w_f(T)) \, |\langle 0, f|\hat{H}_{\mathrm{sb}}|1, i\rangle|^2 \delta(\varepsilon_f - \varepsilon_i - \hbar\omega_0). \tag{41}$$

Here, $|i\rangle$ and $|f\rangle$ are initial and final bath states, and ε_i and ε_f the corresponding energies. Further, $w_i(T)$ and $1 - w_f(T)$ are probabilities that these states are occupied and empty, respectively, at temperature T. Finally, $\hbar\omega_0$ is the fundamental vibrational quantum.

To treat vibrational relaxation by *vibration–phonon* coupling, the bath modes are chosen as phonons or, in a discrete representation, normal modes of a cluster. The system mode q can be harmonic or not, and $\hat{H}_{\mathrm{sb}}$ is often obtained from a Taylor expansion of the total potential:

$$\hat{H}_{\mathrm{sb}} = \sum_k^N f_k(q) Q_k + \sum_{k,l}^N g_{kl}(q) Q_k Q_l + \sum_{k,l,m}^N h_{klm}(q) Q_k Q_l Q_m + \cdots. \tag{42}$$

Here, N harmonic bath vibrations with frequencies ω_k are included. The first, second, third, ... terms on the rhs give rise to one-, two-, three-phonon ... processes, with $f_k(q)$, $g_{kl}(q)$, $h_{klm}(q)$ ... denoting the corresponding coupling functions. In equation (42), the frequencies ω_k and normal modes Q_k can be obtained from normal mode analysis of a large cluster.

If the system mode is approximated as being harmonic, and if only one-phonon terms are included and the coupling function is assumed to be $f_k(q) = \lambda_k q$, one obtains the harmonic, bilinear coupling model for which, at $T = 0$, the transition rates are

$$W_{\alpha\to\beta} = \delta_{\alpha,\beta+1}\alpha W_{1\to 0}. \tag{43}$$

This suggests the strict selection rule $\Delta v = -1$, with a relaxation rate proportional to the quantum number α of the decaying state. The rate $W_{1\to 0}$ at $T = 0$ is equivalent to η_{ph}. At finite temperature, upward rates come into play which obey detailed balance.

The above and related formalisms have been applied to a variety of systems [112, 113]. For example, the decay of the Si–H stretch mode at hydrogen-covered silicon surfaces was investigated by perturbation theory. The experimental lifetime of the first excited Si–H stretch vibration of H:Si(100)2 × 1 at $T = 300$ K is $\tau_{\mathrm{vib}} \sim 1.2$ ns [109], and increases with decreasing temperature to several nanoseconds. In [29, 28], the relaxation of the Si–H vibration was treated within a one-dimensional harmonic-oscillator model along the Si–H distance r, with the lifetime at $T = 0$ entering as an empirical parameter. Since the Si–H stretching mode has a frequency of about 2100 cm^{-1} while the Debye frequency is ∼520 cm^{-1}, it was suggested in [28, 109] that the relaxation proceeds by emission of three Si–H bending vibrations (with about 630 cm^{-1} each), plus one bulk Si phonon.

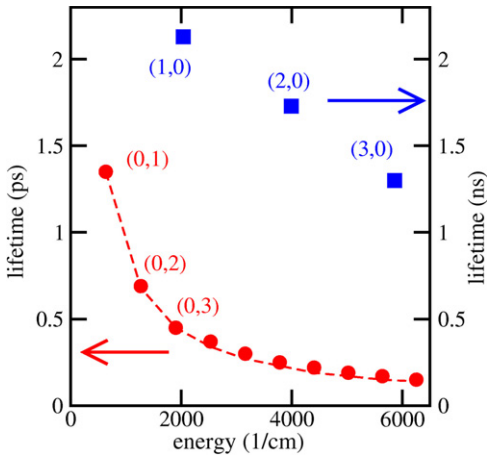

Figure 8. Vibrational lifetimes of selected vibrational states (v_s, v_b) of H/Si(100), at $T = 0$ K. For the calculation, a cluster model consisting of 180 atoms has been used. The left (ps) scale refers to the bending vibrations, the right (ns) scale to the stretching vibrations. See [115] for details.

In [114, 115] a semiempirical bond-order potential [116–118] was used to provide 'absolute' rates for H:Si(100)2 × 1. As a new aspect, two modes were treated non-perturbatively, namely the r mode, and the Si–Si–H bending along the bending angle, ϕ. The system modes were anharmonic, and non-linearly coupled to harmonic surface oscillators, obtained from normal mode analysis of clusters. A lifetime for the stretching mode of H:Si(100) of about 1.5 ns was found at room temperature [114, 115], which increases with decreasing temperature, both findings in reasonable agreement with experiment. Also, higher excited vibrations $v > 1$ and the vibrational relaxation of the bending mode were considered. It was found that, in particular for the bending mode, the decay rates increase approximately according to the simple scaling law (43). It was also predicted that the Si–H bending mode decays on a picosecond timescale. Since $\omega_\phi \sim 630\ \mathrm{cm}^{-1}$, two phonons are required to achieve this.

In figure 8 the vibrational lifetimes of selected vibrational states (v_s, v_b) at $T = 0$ K are shown, where v_s refers to the number of vibrational quanta in the stretch mode, and v_b to the number of vibrational quanta in the bending mode. For the calculation, a cluster model consisting of 180 atoms has been used, as described in [115].

Vibrational damping due to vibration–electron coupling can also be treated perturbatively. Again equation (41) is used for this, where $|i\rangle$ and $|f\rangle$ are now initial and final *electronic* states, with energies ε_i and ε_f, and $w_i = w(\epsilon_i)$ is the probability, according to a Fermi–Dirac distribution, that $|i\rangle$ is occupied at temperature T.

Using a Newns–Anderson-type model Hamiltonian the electronic states entering (41) are the resonance state $|a\rangle$ and the metal states $|k\rangle$. Further, for the coupling operator one may take an operator linear in the system mode, q. Within this model, and making further approximations, Persson and Persson [119] derived expressions for the vibrational damping rate η_{el}, the simplest one being

$$\eta_{\mathrm{el}} = 2\pi\omega_0(\delta n_a)^2. \tag{44}$$

Here, δn_a is the fluctuation of the occupation of acceptor level $|a\rangle$ during one vibration.

This theory is insightful, but for reliable predictions more quantitative expressions are needed. One such approach is due to Tully and Head-Gordon, which is based on an *ab initio*

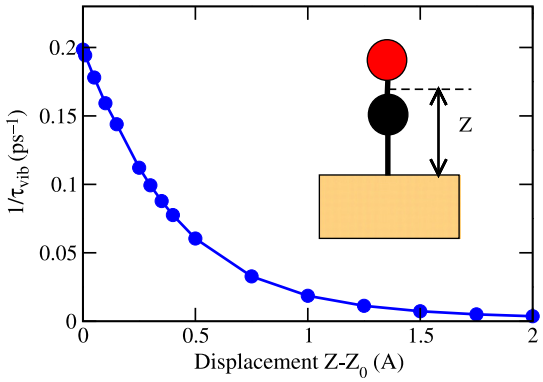

Figure 9. Dependence of the (inverse) vibrational lifetime of the CO ($v = 1$) stretch vibration of CO/Cu(100) on the displacement $Z–Z_0$ from the equilibrium CO–Cu distance Z_0.

quantum chemical cluster model [98, 110, 111]. The starting point is equation (41), with $|i\rangle$ and $|f\rangle$ being electronic wavefunctions calculated from Hartree–Fock orbitals. Further, the coupling operator $\hat{H}_{\rm sb}$ is the kinetic energy operator of the nuclei, $\hat{H}_{\rm sb} = \hat{T}_R$. For a single nuclear mode $R = q$, which is treated as harmonic, and by treating the derivative couplings in an approximate way one obtains [110]

$$\eta_{\rm el} = \pi\hbar\frac{\hbar\omega_0}{m_q}\sum_{n\in{\rm occ}}\sum_{r\in{\rm virt}}\left|\left\langle\chi_r\left|\frac{{\rm d}\chi_n}{{\rm d}q}\right|_0\right\rangle\right|^2\delta(\varepsilon_n - \varepsilon_r + \hbar\omega_0), \tag{45}$$

where χ_n denotes an occupied, and χ_r an empty, Hartree–Fock orbital. Further, the matrix element is a one-electron integral with $\frac{{\rm d}\chi_i}{{\rm d}q}|_0$ denoting the derivative of orbital χ_i at $q = 0$. Head-Gordon and Tully rewrote equation (45) in an LCAO-MO frame, ending up, after a few additional approximations, with an elegant trace formula for $\eta_{\rm el}$. A similar approach, albeit in the framework of periodic DFT, had earlier been taken by Hellsing and Persson [120]. Their method was recently widely used [99, 121–123].

The cluster approach of Tully and Head-Gordon has been applied, within Hartree–Fock theory, to vibrational damping of CO/Cu(100) [98, 110, 111]. Typical cluster sizes were CO/Cu_6, CO/Cu_{10}, and CO/Cu_{14}. In particular, the ps lifetime of the CO ($v = 1$) stretch mode was well reproduced.

We have implemented the Tully/Head-Gordon theory to calculate the dependence of the CO ($v = 1$) lifetime, on the molecule–surface distance, Z. Using a cluster Cu_6–CO, the same double-ζ basis set and effective core potentials as in [110, 111], and Hartree–Fock theory, the vibrational lifetime was found to increase exponentially with Z, as demonstrated in figure 9. It is found, within this particular cluster and computational model, that the lifetime decreases from about 5 ps at $Z = Z_0$, to about 50 ps when the CO molecule is displaced from its equilibrium position, by about +1 Å.

2.5.2. Electronic relaxation. For metal surfaces with adsorbate lifetimes as short as femtoseconds, quantum mechanical calculations of $\tau_{\rm el}$ and hence Δ_a are still rare. In [124], a tight-binding Green's function method was proposed, in which a Dyson equation

$$\underline{\underline{G}}(E) = \left(\underline{\underline{1}} - \underline{\underline{G}}^0(E)\underline{\underline{V}}\right)^{-1}\underline{\underline{G}}^0(E) \tag{46}$$

is solved. Here, $\underline{\underline{G}}^0 = (E\underline{\underline{1}} - \underline{\underline{H}}^0)^{-1}$ is an unperturbed, block-diagonal Green's matrix for an isolated adsorbate far from an infinite surface, derived from the interaction-free Hamiltonian

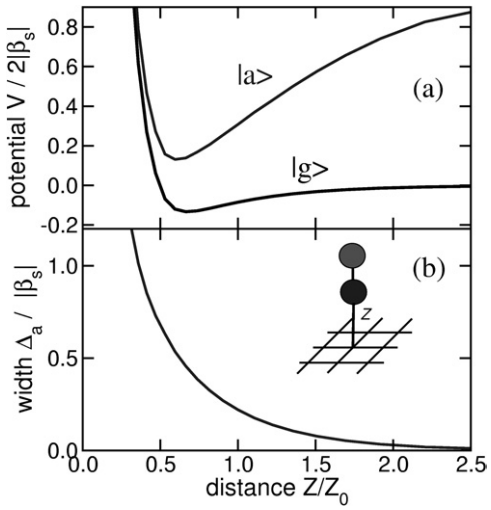

Figure 10. Results from a tight-binding Dyson equation approach [124] to the binding of a diatomic molecule on a (100) surface (inset of (b)). Shown are the potential energy curves for the ground state and a (negative ion resonance) excited state (a), and the resonance width Δ_a, as a function of molecule–surface distance (b). Units are in $2|\beta_s|$ for energies and $|\beta_s|$ for the width, where β_s is the tight-binding parameter for the metal–metal interaction, and Z_0 a reference distance as defined in [124]. Further tight-binding parameters and details of calculation are also described in [124].

$\underline{\underline{H}}^0$. $\underline{\underline{V}}$ is the coupling between molecule and surface at finite distance, and $\underline{\underline{G}}$ the corresponding perturbed Green's matrix. Solving (46) at energy $E^+ = \lim_{\eta\to 0}(E + \mathrm{i}\eta)$ gives the density of states according to

$$\rho(E) = -\frac{1}{\pi}\mathrm{Tr}\{\mathrm{Im}\,[\underline{\underline{G}}(E^+)]\}. \tag{47}$$

By projecting the latter on the adsorbate level(s) of interest, one obtains the local density of states ρ_a whose width is the resonance width, Δ_a. The method was used to estimate the lifetime of the negative ion resonance of a diatomic molecule on a metal surface. With 'typical' tight-binding parameters representing an Antoniewicz-type situation similar to that applying to NO/Pt(111) (i.e., a single electron is transferred from the surface to the molecule), a lifetime in the femtosecond range is found at the equilibrium bond length. This lifetime increases exponentially with molecule–surface distance, Z, as indicated in figure 10. The method should be extendable to the *ab initio* world. Similar methods, in part already based on 'first principles', have been used in [125–127].

Excited state 'lifetimes' can also be estimated by solving equation (7) from coupled nuclear wavepackets, or, equivalently, by solving the electron–nuclear Schrödinger equation (8). The decay of an initial wavepacket in front of a surface can be non-exponential, in particular if the substrate is a metal. Such approaches have been used in [50–52]. As an example, we demonstrate in figure 11 the decay of a NO^- resonance in front of a thin Pt(100) film. The two-dimensional electron–nuclear model potential $V(x, Z)$ of figure 5 was used, and the Schrödinger equation (8) solved, as a diabatic multi-state model. What is shown is the square modulus of the autocorrelation function $C(t)$, with

$$C(t) = \langle\psi(x, Z, t)|\psi(x, Z, 0)\rangle_{x,Z}. \tag{48}$$

The initial wavefunction $\psi(x, Z, 0)$ was entirely localized in the NO^--like potential well at $x \sim 2a_0$ and $Z \sim 1.7a_0$ (see figure 5), generated as described in [51]. From the decay of $|C(t)|$

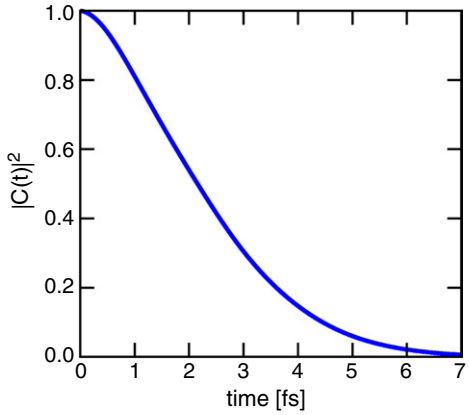

Figure 11. Decay of a NO^- resonance state, for NO in front of a Pt film 30 a_0 (∼16 Å) thick. See text and [51] for details.

due to tunnelling into the bulk, a resonance lifetime in the order of a few femtoseconds can be anticipated for NO/Pt.

A similar approach, based on three-dimensional electronic wavepacket propagation, was taken in [128–130], to explain the unusual long lifetime [131, 132] of an antibonding state ('A state') of alkalis such as Cs on copper surfaces.

3. Photodesorption of atoms and molecules from semiconductor and metal surfaces

3.1. Hydrogen desorption from Si(100)2 × 1

The desorption of H and D from hydrogen-covered Si(100)2 × 1 can be enforced with an STM but also with UV photons [12]. The photons or tunnelling electrons enforce a direct $\sigma \rightarrow \sigma^*$ transition [12]. Here, $V_\sigma = V_g$ refers to a ground state, which is bound by about 3.4 eV along the H–Si distance r, and $V_{\sigma^*} = V_a$ to an excited, repulsive state. Based on MCSCF cluster calculations Avouris and co-workers constructed potential curves $V_g(r)$ and $V_a(r)$, to explain their 'above threshold' STM experiments at sample bias voltages of >7 V [26]. The *ab initio* based model potential curves are qualitatively analogous to those of figure 4(a), i.e. an MGR-type situation is found. A semiclassical variant of Gadzuk's jumping wavepacket algorithm was used to rationalize the unusual large isotope effect in the yields,

$$R = \frac{Y(H)}{Y(D)} \tag{49}$$

of about 50. To do so, an ultrashort lifetime of the excited state of $\tau_{\mathrm{el}} \sim 0.5$ fs was assumed. The short lifetime arises from the fact that the $\sigma \rightarrow \sigma^*$ excitation lies in the conduction band of the Si surface. As a result of the short lifetime, desorption probabilities are very small. For H the yield is about 10^{-4} per excitation event, and for the heavier D correspondingly smaller, causing the large isotope effect.

The same model and method was adopted by Vondrak and Zhu to explain their UV desorption experiment, with a similarly large isotope effect [12]. In [133] and [134], effects of an (exponential) coordinate-dependence of the quenching rate $W^{\mathrm{el}}_{a\rightarrow g}(Z)$ were considered in addition. The calculations were based on a two-state model and open-system density matrix theory, i.e. solution of equation (17), without direct couplings $\tilde{V}_{\sigma\sigma^*}$, and an initial density operator $\hat{\rho}_0 = |\sigma^*\rangle\langle\sigma^*| \otimes |\phi_0^\sigma\rangle\langle\phi_0^\sigma|$. For related theory on this system, see [135–137].

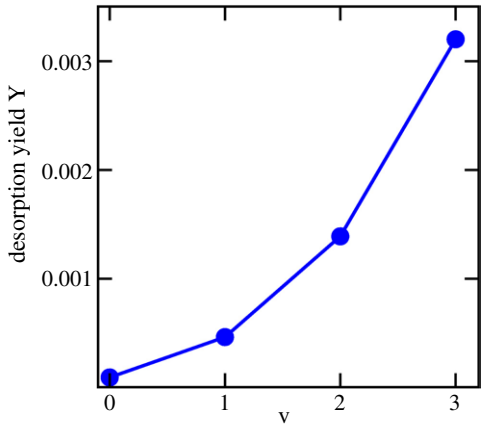

Figure 12. DIET of H from H/Si(100): dependence of DIET yield on vibrational quantum number, v, of the Si–H stretch mode, prior to electronic excitation. An electronic lifetime $\tau_{el} = 0.45$ fs was assumed.

Since, on the one hand, the DIET probabilities are small for H/Si(100), and on the other hand the vibrational lifetimes of the H–Si stretching modes are large, one may speculate that IR excitation of the Si–H bond prior to the electronic excitation will lead to a substantial increase of the desorption yield. This IR+UV strategy is known as 'vibrationally mediated chemistry' [138–140]. For desorption of H/Si(100), it is demonstrated in figure 12 that the desorption probability can indeed be dramatically enhanced, when instead of $|\phi_0^\sigma\rangle$, a vibrationally excited eigenstate $|\phi_v^\sigma\rangle$ is Franck–Condon excited to V_{σ^*}. Also, IR laser pulses have been designed for selective excitation of the Si–H vibration, using an iterative scheme and one- and two-dimensional model potentials and dipole functions for the Si–H bond [141].

It was also suggested that IR pre-excitation will not only lead to larger desorption yields, but may also be used for isomerization reactions [142, 143], and for isotope-selective chemistry [144, 145]. Further, since in PSD of H/Si(100) the electronic excitation is direct, shaped UV laser pulses could also be useful to control the reaction [134]. In [134] it was numerically demonstrated that ultrashort pulses would indeed enhance the desorption probability substantially.

3.2. Photodesorption of NO from Pt(111)

3.2.1. DIET. NO desorption from Pt(111) is a prototype system for substrate mediated DIET. Also for this system representative, dissipative two-state models of the type used in equation (17) have been devised. These models are either one dimensional, with the desorption coordinate, Z, being the one mode considered [67, 68, 146, 147, 87, 88, 148–152], or two dimensional, either with Z and the NO distance r [90, 91, 153–156], or Z and polar angle θ [157, 158] included. The 2D (r, Z) model has also been used for nonadiabatic scattering of NO from Pt(111) [159].

Model potentials were developed for the ground state V_g and the negative-ion resonance state V_a. In the 1D models, the ground state was chosen as a Morse potential, and the excited state as a negative ion resonance potential [87]:

$$V_a(Z) = V_g(Z) + \Phi - \mathrm{EA} - \frac{e^2}{4Z}. \tag{50}$$

For $Z \to \infty$ this potential accounts for the energy difference between ionic and neutral (ground) state, through the work function Φ of the metal and the electron affinity EA of the

molecule. Closer to the surface the ionic state is stabilized by image charge attraction, the last term in equation (50). As a consequence, a photoexcited adsorbate moves initially inward according to an Antoniewicz model, as indicated in figure 4(c).

In the dissipative two-state models, the excited state lifetime was chosen semi-empirically in most applications so far, with $\tau_{\rm el} \sim$ 2–10 fs, depending on model and reference. The substrate-mediated excitation process was treated by a singular Franck–Condon transition of the ground state vibrational wavefunction to the excited state.

After applying nanosecond laser pulses for electronic excitation, a striking experimental observation for NO/Pt(111) was that the molecules come off the surface vibrationally hot [13, 14]. The vibrational state distribution $P_{\rm v}$ was almost Boltzmann, with a vibrational temperature $T_{\rm vib} \sim 850$ K. This was again attributed to the assumption that during desorption an anion state is temporarily populated, in which the NO bond is stretched [153, 155]. However, by assuming in simulations a bond elongation of $\Delta r \sim 0.1$ Å as for a free NO^- ion led to much larger vibrational excitation than actually observed [160]. In fact, with this assumption a population inversion of vibrational levels is predicted, while according to experiment only the lowest two levels are significantly populated, with a ratio $P_1/P_0 \sim 0.04$. A number of possibilities, among them only partial charge transfer to NO, and a quenching rate $W^{\rm el}_{a\to g}$ that is coordinate dependent, have been discussed [90] to resolve this issue.

Another possible reason for the smaller than expected vibrational excitation of the desorbing molecule is vibrational relaxation of the NO bond near the surface. As can be seen from figure 9, for example, the quenching of internal adsorbate modes by vibration–electron coupling can in fact be very efficient when the molecule is close to the substrate. This possibility was investigated in [154] within the two-state (r, Z) model. The vibrational lifetime of the NO bond was estimated from *ab initio* cluster calculations, with the simplified expression (44), as $\tau_{\rm vib} \sim 500$ fs. It was found that vibrational relaxation of the NO bond lowers the desorption probability, and favours $v = 0$ for desorbing NO(v) in expense of higher v. Thus, vibrational cooling of the NO bond may help to explain the observed, relatively moderate vibrational energy of desorbing NO [13, 14]. In passing we note that a similar vibrational excitation was found for NO desorbing from NiO(100) [161], and explained with similar arguments and models as those above [162–167].

The vibrational relaxation of the NO–Pt bond was the subject of two other studies [156, 71]. The vibrational lifetime was empirically chosen to be several picoseconds in both references, in accordance with findings for similar systems [98]. In [156] a special Lindblad-type relaxation operator, with the NO–Pt bond treated in the harmonic approximation, was used. In [71], anharmonic raising and lowering operators as described in [69–71] were adopted instead. NO–surface relaxation led again to a reduction of the desorption probability of several per cent, and, more importantly, to a saturation of Y, which is often not reached in finite-time propagations without vibrational relaxation. The calculated desorption probability itself is small, $\sim 10^{-4}$ per absorbed photon in the 1D model with $\tau_{\rm el} = 2$ fs [68].

In the above applications, the dissipative two-state model of section 2.3.1 was employed, with the need to use an (empirical) excited state lifetime, $\tau_{\rm el}$. Also, the excitation was treated as a Franck–Condon transition, with details of the laser pulse unaccounted for. Both of these restrictions can be overcome by adopting the nuclear–electron wavepacket method described in section 2.2.

Using slab geometries and the extended close coupling scheme to generate problem-adapted diabatic states from the model potential $V(x, Z)$ of figure 5, the photodesorption of NO from thin Pt films was studied in [51]. In effect, a special variant of the coupled multi-state model in figure 4(b) was used, with a ground state $|g\rangle$, and adsorbate state $|a\rangle$, metal states $|k\rangle$, and non-Born–Oppenheimer and dipole couplings between them. The thicker the films, the

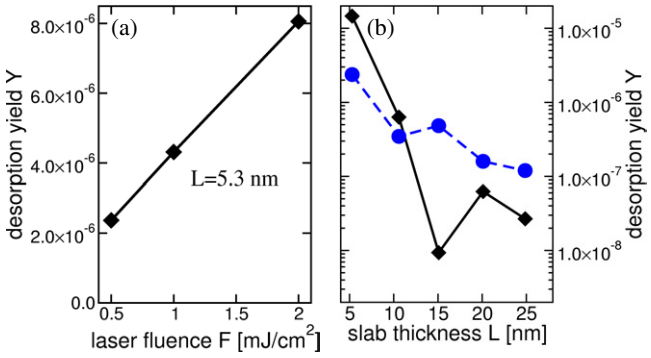

Figure 13. DIET of NO from Pt films, treated within the coupled nuclear–electron model. $\sin^2$ laser pulses with $\sigma = 80$ fs were used in all cases. (a) Dependence of Y on laser fluence, F, when the laser carrier frequency was $\omega = \omega_{\rm res}$, for a film with thickness $L = 5.3$ nm. (b) Dependence of Y on film thickness, L, for $F = 0.5$ mJ cm^{-2}, when either $\omega = \omega_{\rm res}$ (dashed, circles), or $\omega = 2\ eV/\hbar$ (solid, squares) were chosen. See [51] for details.

more metal excited states come into play. As an initial state, the vibrational ground state on the adiabatic ground state potential was used, multiplied by a Bloch state close to the Fermi level. Using laser pulses

$$E(t) = E_0 s(t) \cos(\omega t) \tag{51}$$

with a shape function $s(t)$ of $\sin^2$ form and with a width $\sigma = 80$ fs, it is demonstrated in figure 13(a) that within a fluence range up to $F = 2$ mJ cm^{-2} the desorption yield increases linearly with laser fluence. This implies a DIET regime, mostly because in the one-electron picture no other process is possible. There is also a pronounced dependence of Y on the laser frequency ω, with enhanced (but not necessarily maximal) reaction probability around $\omega = \omega_{\rm res}$, where $\hbar\omega_{\rm res}$ is the energy difference between $|g\rangle$ and $|a\rangle$, at equilibrium NO–surface distance Z_0. For a film 5.3 nm thick, $\hbar\omega_{\rm res} \sim 2.4$ eV. Finally, there is a clear dependence of Y on the film thickness, L, as demonstrated in figure 13(b). As a major trend one observes that the reaction probability increases with decreasing film thickness by one to two orders of magnitude when going from $L = 25$ to 5.3 nm. This appears to be due to larger transition dipole moments for the thinner films in the present model, which favours the formation of a negative-ion resonance. In general, several other mechanisms for the enhancement of the photoreactivity in nanostructured materials are possible, for example (discontinuous) variations in the metal density of states and the resonance lifetimes [126, 168, 169].

3.2.2. DIMET. Femtosecond laser induced desorption is interesting for many reasons, in particular due to the possibility of DIMET. One of the first systems for which DIMET has been observed is NO/Pd(111), with a nonlinear scaling of the yield versus fluence according to equation (2) [16]. This DIMET hallmark, and several others, were reproduced and explained in [17], with stochastic trajectory simulations using two-state models. The stochastic trajectory method is the classical analogue to the quantum mechanical DIMET model based on open-system density matrix theory of section 2.3.2, when realized by an MCWP algorithm [146]. The classical particles undergo random jumps between the neutral ground state potential $V_g(Z)$ and the anion state $V_a(Z)$, and vice versa. The jumps are governed by the upward rate $W^{\rm el}_{g\to a}$, which depends on the time-dependent electronic temperature $T_{\rm el}(t)$, and the downward rate $W^{\rm el}_{a\to g} = \tau^{-1}_{\rm el}$. For the latter $\tau_{\rm el} = 2$ fs was assumed in [17], and $T_{\rm el}(t)$ calculated from the two-temperature model.

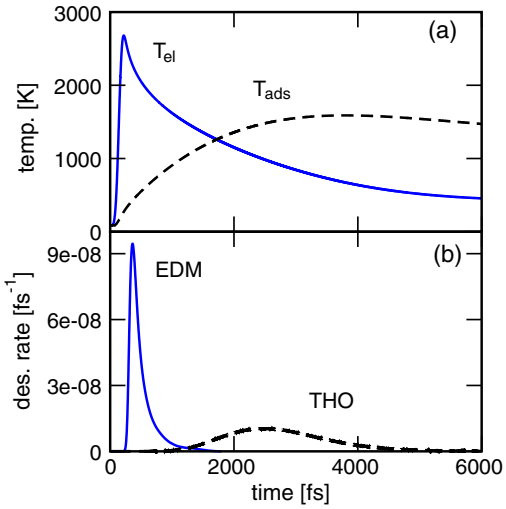

Figure 14. DIMET of NO from Pt with the same 80 fs laser pulse as used in figure 6(a). In the upper panel (a) $T_{el}(t)$ is shown again, now in comparison to the vibrational temperature T_{ads} of the electronic friction/THO model. In the lower panel the desorption rates $R_{des}(t)$ are given for the THO and the excitation–de-excitation models (EDM). See [71] for details.

The fully quantum mechanical open-system density matrix approach was applied in [67, 68, 71, 151] for FLD of NO/Pt(111), within one- (r), and in [90, 91] in two-dimensional (r, Z) models. Also for this system $\tau_{el} = 2$ fs was assumed (in the 1D model), and the 2TM was used to get the upward rate in equation (25). The LvN equations were solved either by direct density matrix propagation [68], by stochastic wavepacket methods [91, 146], or by a variational wavepacket method [170]. The stochastic wavepacket approach is useful to quantify the notion of 'multiple' in DIMET. As a result, for realistic $T_{el}(t)$ profiles it was found that the average number M of excitations per pulse is surprisingly small [68]. In many cases none or only a single excitation takes place. This is consistent with an independent analysis of Gadzuk [171].

Again the non-linear scaling law (2) could be reproduced [71, 151]. A scaling exponent in equation (2) of $n \approx 4.4$ was found, in reasonable agreement with the experimental value of $n = 6 \pm 1$ [19]. In contrast, the THO model based on the electronic friction concept [102], and Arrhenius equations of the type (33), overestimated this value [71].

In [71], besides electronic relaxation, vibrational relaxation of the NO–surface mode was accounted for, leading to a (small) reduction of the desorption yield also in DIMET. In [71] it was further found, based on calculation of the vibrational state distribution $P_v(t)$ of the NO–substrate vibration from the full density matrix, that $P_v(t)$ is nonthermal, for at least several hundred femtoseconds. This renders the notion of an adsorbate vibrational temperature T_{ads} as used in Arrhenius expressions like (33) somewhat questionable.

A further difference between the electronic friction models, which can be classified as 'weakly nonadiabatic', and the more 'strongly nonadiabatic' excitation–de-excitation models, refers to the predicted *timescales* of desorption. In the electronic friction models, the timescale of desorption is determined by the electronic friction coefficient, $t_{des} \sim \eta_{el}^{-1}$. This is typically several picoseconds. In the excitation–de-excitation models, on the other hand, the timescale for desorption is determined by the rise time of $T_{el}(t)$, i.e. typically a few hundred femtoseconds. This is illustrated in figure 14, where it is shown that the desorption rate R_{des} in

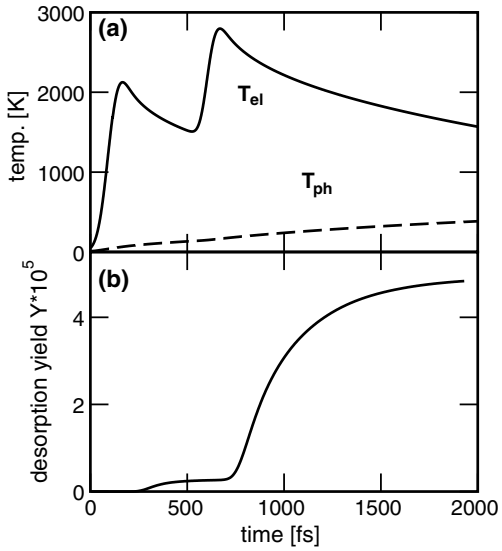

Figure 15. (a) Electron and phonon temperatures T_{el} and T_{ph} following two identical laser pulses with $F = 4.5$ mJ cm^{-2}, FWHM = 80 fs, and delay $\Delta\tau = 500$ fs, according to the two-temperature model. (b) Corresponding desorption yield Y. See [71] for details.

the excitation–de-excitation model follows $T_{el}(t)$, while it follows the retarded $T_{ads}(t)$ curve in an electronic friction model, such as THO. For FLD of CO from copper a timescale of <325 fs has been measured by SHG pump–probe experiments [20]. This is shorter than predicted by the friction models, a shortcoming of the latter that had been realized earlier [20, 101].

The predicted, more rapid desorption is also the reason why, at least in single-pulse DIMET, vibrational relaxation is considered (and found) less important when excitation–de-excitation models are used [71]. In contrast in the friction models, an infinite vibrational lifetime would correspond to a vanishing desorption rate (see equation (33)), because electron–vibration coupling is essential both for FLD and vibrational relaxation. This latter, attractive feature is missing in the excitation–de-excitation models, while others—such as the details of the topology of the excited state potential and consequences resulting thereof—are missing in current electronic friction models. Thus, none of the existing models of FLD appear to be 'complete' in the authors' opinion.

3.2.3. Time-resolved spectroscopy: 2PC traces. As mentioned earlier, 'phononic' versus 'electronic' mechanisms of FLD and related reactions are frequently discriminated by two-pulse correlation (2PC) traces. Again for NO/Pt, 2PC traces of desorption yields were calculated, using the 1D two-state density matrix model in combination with the two-temperature model [71]. In figure 15(a) we show the electronic temperature $T_{el}(t)$, according to the 2TM, when two identical laser pulses delayed by 500 fs are used. Due to the nonlinear dependence of the yield on the electron temperature, a desorption probability increase much larger than by a factor of two can be achieved, as demonstrated in figure 15(b).

The computed 2PC signal $Y(\Delta t)$ falls off rapidly initially, on the timescale of a few hundred femtoseconds [71]. This is indicative of an electronic mechanism. It was also found, however, that the initial steep decay of $Y(\Delta t)$ is followed by a long tail extending far into the picosecond and, probably, even nanosecond regime. Nevertheless, in this regime

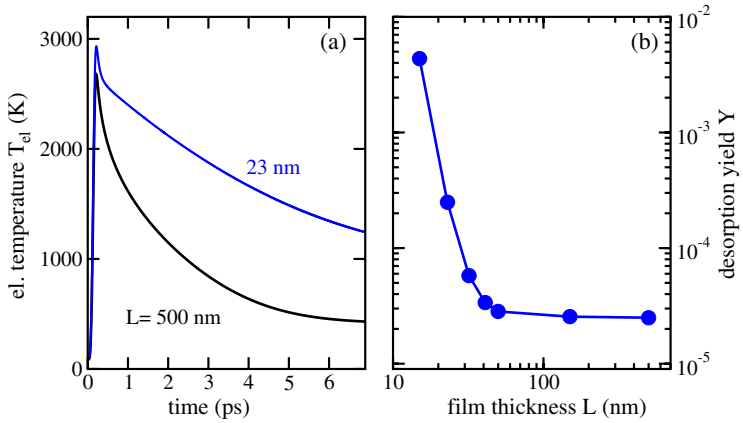

Figure 16. (a) $T_{el}(t)$ curves for a Pt film, 500 nm thick (indistinguishable from the bulk), and a film only 23 nm thick. A Gaussian laser pulse polarized perpendicular to the substrate was used with fluence $F = 6$ mJ cm^{-2}, FWHM = 80 fs, and $\lambda = 619$ nm. (b) Desorption yields resulting from the open-system density matrix model, for different film thicknesses L [151].

the mechanism is also still purely electronic. This follows from the simple fact that in our model no phononic mechanism was accounted for. The reason for this behaviour is in the two-temperature model, which predicts a fast decay of $T_{el}(t)$ due to electron–phonon coupling, followed by a slow decay as soon as $T_{el} \approx T_{ph}$, when diffusive cooling begins to dominate. As a consequence, the second pulse finds the electrons hot for long times, leading to larger yields than one would expect for two uncorrelated laser pulses. This finding suggests that the classification as 'phononic' or 'electronic' mechanisms from timescale arguments alone is not entirely straightforward.

3.2.4. Controlling surface reactivity. For 'hot-electron' mediated femtosecond laser chemistry, the yield not only depends on fluence, but on other external parameters as well. An example is, in the case of metal films, the film thickness, L. The confinement has an influence on the $T_{el}(t)$ curve, as demonstrated in figure 16(a). We find according to the 2TM with a thickness-dependent source term $S(t)$ as in equation (29) that with decreasing film thickness the maximum electronic temperature, T_{el}^{max}, increases. From figure 6(b) we recall that $T_{el}^{max} \propto \sqrt{F}$; now, one finds in addition an approximate relation $T_{el}^{max} \propto \sqrt{1/L}$. This suggests that lowering L has a similar effect to increasing F. In figure 16(a) it is also observed that the electronic temperature remains high for a longer time in thin films, before heat diffusion cools the electrons. As a consequence, the hot-electron mediated desorption depends sensitively on film thickness, which is demonstrated in figure 16(b). The mechanism by which this occurs, namely through the hot-electron temperature profile, is, however, different from the mechanism suggested previously for DIET (see figure 13(b)).

There are also attempts to control surface photoreactivity in FL experiments by the light source itself. A difficulty arising for substrate-mediated photochemistry is that the adsorbate is excited only indirectly, i.e. *coherent control* is not easily possible. *Incoherent control*, on the other hand, by 'controlling' the hot-electron temperature $T_{el}(t)$, is not only possible through variation of F or L. In [151] it was shown that the *shape* of the laser pulse envelope is also a possible 'control' parameter. This is in agreement with an experimental finding for FLD of CO/Pt(111), where the yield depends on whether shorter or longer femtosecond pulses are used [173]. A theoretically predicted controllability of FL desorption by chirped pulses [172],

on the other hand, could not be supported by experiment: chirping had no effect on the desorption of CO/Pt(111) [173].

While UV/vis photons penetrate most metal surfaces, thus favouring hot-electron mechanisms, IR photons couple directly to the adsorbate–surface bond. Thus, the IR+UV/vis strategy mentioned above for H/Si(100) has also been suggested to be useful for metal surfaces, where, however, the electronic excitation is an incoherent process [67, 68, 133, 134, 144, 145, 152, 174]. From DIMET it is known that vibrational excitation favours desorption. This is also consistent with experimental findings for DIET, where vibrational enhancement was achieved by simple surface heating [162, 175, 176]. When using IR pulses in the picosecond domain instead, of Gaussian or $\sin^2$ shape, for example, state-selective excitations should be possible. Only recently optimal control theory was also adopted for this purpose [152, 177].

In [152], a hybrid quantum control scheme was applied to NO/Pt(111). In this scheme the NO–Pt bond was coherently excited with IR pulses obtained from optimal control theory, before incoherent electronic excitation by hot electrons sets in. The same one-dimensional two-state model within open-system density matrix theory with Lindblad excitation/de-excitation operators [68] was used as above. The optimal IR pulse prepares the NO molecule such that it moves towards the surface by the time when the hot-electron excitation is maximal. By this preparation the Antoniewicz mechanism is enhanced, and desorption yields an increase by a factor of about eight.

4. Related processes

4.1. Hydrogen switching on H:Si(100)2 × 1

As soon as with an STM (single) hydrogen atoms were desorbed from a H:Si(100)2 × 1 surface [26, 30], a Si dimer with one H atom and one 'dangling' bond is left, as indicated in figure 17(a). It was shown [31, 32] that with an STM operating at negative sample bias the remaining H atom can laterally be switched back and forth between the dangling bond site and its original position. A large isotope effect was found for the switching probabilities, $P_{\rm sw}(H)/P_{\rm sw}(D) \sim 7$. In contrast to previous atom switches on metal surfaces [178–181], the H atom forms a strong chemical bond to the surface, and ground state switching would require a large activation energy of more than 1 eV.

Because of this large barrier, it was conjectured in [31, 32] that H switching on Si(100) requires electronic excitation. A one-dimensional two-state model was devised [31, 32], with ground and excited state potentials $V_g(x)$ and $V_a(x)$. Here, x is a 'switching coordinate' along the Si dimer (figure 17(a)). The potentials were constructed from periodic DFT calculations. Both potentials are double minima, with 'left' and 'right' wells corresponding to stable positions of a single H atom on a Si dimer, as shown in figure 17 (left panel). The excited state, about 2.7 eV above the ground state, is a short-lived 'resonance' with a diffusion barrier much smaller than in the ground state. The lifetime of the resonance was estimated as $\tau_{\rm el} \sim 2.5$ fs.

In [142] this two-state model was adopted within open-system density matrix theory. The 'above threshold' STM excitation was treated as in STM-DIET, by a singular Franck–Condon transition of a wavepacket that was localized in the left well initially. In deviation from [31, 32], it was found that the switching occurs in the ground state, not in the excited state, after rapid electronic quenching. However, the switching in the ground state happens close to the barrier top, thus explaining the non-vanishing switching probability and the isotope effect. In contrast to photodesorption, the vibrational relaxation in the ground state cannot be neglected and both $\tau_{\rm el}$ and $\tau_{\rm vib}$ must be included. Otherwise a rate cannot be properly defined,

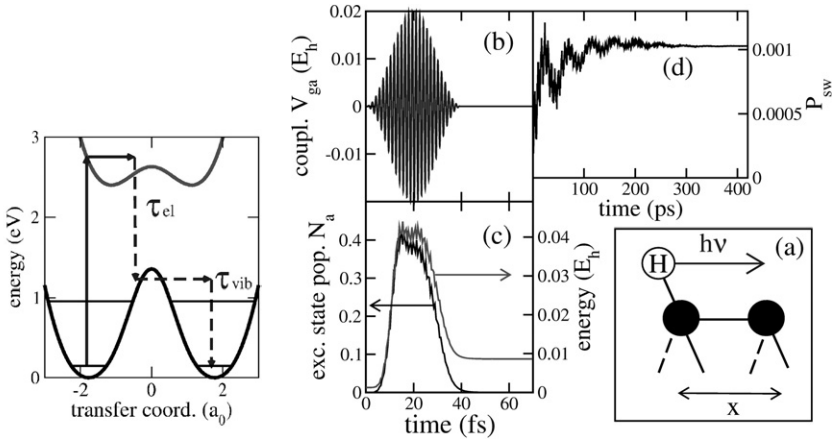

Figure 17. Laser-induced switching of a H atom on a Si_2 dimer of Si(100). Left: model potentials, with excitation and relaxation pathways indicated. Right: (a) schematic illustration of the switching process; (b) field coupling matrix element $V_{ga} = -E(t)\mu_{ga}$ for the direct $|g\rangle \rightarrow |a\rangle$ transition, for a 20 fs pulse. Energies are in Hartree, 1 $E_h = 27.21$ eV. Assuming $\mu_{ga} = 1$ ea_0, this would correspond to a fluence of about 8 mJ cm^{-2}. (c) Corresponding time-resolved excited state population, N_a, and total system energy. (d) Time-resolved switching probability. An excited state lifetime $\tau_{el} = 2.53$ fs was assumed, and $\tau_{vib} = 1$ ns. After [154], where further details can be found.

because population would oscillate between left and right wells indefinitely. The timescale for switching is determined by the vibrational lifetime, τ_{vib}, and is therefore 'long'.

In [142] the possibility was also investigated to directly excite the H–Si–Si moiety with 2.7 eV photons. For this purpose femtosecond laser pulses with $\sin^2$ shape were considered, and full widths at half maximum ranging from 20 to 120 fs. As a result, laser switching seems more efficient in comparison to STM switching. This is illustrated in figures 17(b)–(d), showing a representative laser pulse, the resulting excited state population and total system energy, and the switching probability, respectively. For a fixed pulse width of 20 fs, the switching probability increases approximately linearly with laser fluence, up to a fluence of about 8 mJ cm^{-2} [142]. For higher fluences, the switching probability drops, probably due to stimulated emission. A large influence of the switching probability on the pulse length was found. Further, the switching probability, which is about 10^{-3} per pulse in figure 17, was predicted to increase substantially upon vibrational excitation of the bending mode.

4.2. Electron stimulated desorption of CO from Ru(0001)

Electron stimulated desorption as illustrated in figure 2(b) can be described by jumping wavepacket models analogous to DIET, with an initial, impulsive excitation. An example is the ESD of carbon monoxide from Ru(0001) by 150 eV electrons [42, 43], which was studied theoretically in [182] and [183].

In contrast to the 'mild' conditions considered so far, high energy electrons probably lead to a double excitation of the adsorbed CO molecule [42]. As a consequence, not only vibrational excitation, but in fact a vibrational population inversion for the desorbing molecule, was found experimentally, with a maximum around $v = 30$. The possibility of molecular dissociation was conjectured [42].

In [182, 183] a two-dimensional two-state model was developed with Z, the CO–surface distance, and the C–O distance, r, i.e. desorption and dissociation mode. The excited state was

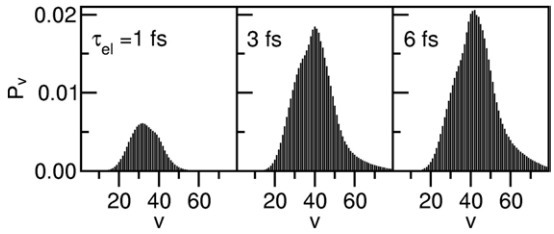

Figure 18. Vibrational state distributions P_v for CO desorbing from Ru(0001), for three different excited state lifetimes τ_{el} [182].

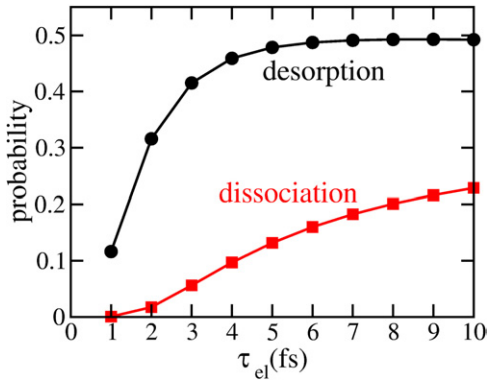

Figure 19. ESD of CO/Ru(0001). Shown are the desorption probability and the dissociation probability as functions of the excited state lifetime. After [182].

assumed to be the $3\sigma^{-1}\ 4\sigma^{-1}\ 2\pi^{+2}$ doubly excited state. Since the latter has two electrons in a C–O antibonding orbital, a strongly elongated C–O bond, and also enhanced CO–surface distance is expected, and found in DFT calculations [184]. After Franck–Condon excitation and subsequent relaxation, the molecule desorbs with substantial vibrational energy, as illustrated in figure 18. In the figure, the population P_v of the 79 bound vibrational states of the desorbing CO molecules is shown. The vibrational excitation is a consequence of the pronounced bond lengthening in the doubly excited state, of about $\Delta r \sim 0.6$ Å. The excited state lifetime is essentially unknown, and was assumed to be in the few femtosecond range. In the figure, three different lifetimes, $\tau_{el} = 1$, 3, and 6 fs, are considered. The $\tau_{el} = 1$ fs lifetime shows a maximum of P_v around $v = 30$, which seems therefore in best agreement with experiment. However, longer or even shorter lifetimes cannot be excluded from the present analysis. From the figure it is also evident that the desorption probabilities increase with increasing lifetime.

According to the model, it is very likely that some of the molecules dissociate after electron impact. The exact number depends on the excited state lifetime. In figure 19 the dissociation and desorption probabilities are shown as a function of lifetime, τ_{el}. For lifetimes $\leqslant$3 fs or so, the dissociation probability is in the order of a few per cent. It is found that in contrast to mild PSD conditions (low energy photons) the desorption probabilities are substantial, $Y \sim$ 0.1–0.5 per excitation, for realistic lifetimes. This is also in agreement with experiment [42]. Both processes, desorption and dissociation, proceed on a femtosecond timescale—therefore vibrational relaxation can be neglected in modelling. Since also much more energy is gained by the wavepacket in comparison to 'ordinary' DIET, there is no substantial dependence of the results on the initial state—all results above are for the vibrational ground state.

4.3. Time-resolved 2PPE spectra of solvated electrons in ice layers on Cu(111)

Lifetimes and timescales in ultrafast surface photochemistry can be unravelled by time-resolved spectroscopy. As an example in figure 3 the probing of an adsorbate resonance state after laser-pulse driven charge transfer from the metal surface by TR-2PPE was illustrated. Additional information is gained by detecting the photoemitted electrons under various observation angles, i.e. by AR-2PPE (angle-resolved 2PPE) [185–187].

Recently, time- and angle-resolved ultrafast two-photon photoemission spectroscopy [188–190] was applied to the problem of electron solvation in polar adsorbate/surface layers. In [189, 190] the electron solvation in ultrathin ice layers deposited on a Cu(111) surface was studied. In the experiment a first (pump) laser pulse excites an electron from below the Fermi level of the copper substrate into the unoccupied ice conduction band, from which it relaxes into a localized state in the ice layer. This is therefore a model reaction for laser-induced electron transfer from a metal to an adsorbate. The localized electron is excited by a second (probe) pulse, acting after a delay time, $\Delta\tau$, above the vacuum level. The ejected electron is detected with respect to its kinetic energy E_{kin} and momentum component parallel to the surface. The electrons can also travel back into the metal, remaining unobserved. As suggested by Harris *et al* for other dielectric layers on metal surfaces [188, 191, 192], the angle-resolved 2PPE signals directly map the projected electron density $|\psi(k_x)|^2$ in momentum space, where $\hbar k_x$ is the electron's parallel momentum, from which the spatial extent of electron localization can be obtained by Fourier transformation. Thus,

$$\Delta x_{\mathrm{ini}} \cdot \Delta k_{\mathrm{fin}} = \text{constant}, \tag{52}$$

where Δx_{ini} is the lateral width of the electron wavepacket prior to the probe pulse, and Δk_{fin} its spread in momentum space, also parallel to the surface. By measuring the latter by AR-2PPE, the size of the electron wavepacket can be determined.

In [193] time- and angle-resolved 2PPE spectra of the ice/Cu(111) interface were simulated by an electronic wavepacket model. For the H_2O/Cu(111) system a two-dimensional Cu slab 'sandwiched' between two isotropic ice layers was considered. Both the electron coordinate normal to the surface, z, and a direction parallel to the surface, x, were accounted for. The total potential consists of two parts: a delocalized electron potential $V(z)$, which is corrugated inside the surface and accounts for the electronic structure of Cu(111) [194, 195] modified with the dielectric continuum potential in the regions of the ice layer and the vacuum [196], plus an empirical potential well for the solvated electron, $V_{\mathrm{s}}(x, z)$, outside the surface, $V(x, z) = V(z) + V_{\mathrm{s}}(x, z)$. The lateral width of the potential well is determined by a width parameter σ_x, its depth by a parameter V_0. Both are varied below to account for the range of binding energies E_{s} of the solvated electron as determined by energy-resolved 2PPE spectroscopy. The situation is schematically illustrated in figure 20. Details of the model potential can be found in [193].

Starting with an electron localized in the potential well, the probe pulse $E_{\mathrm{pr}}(t)$ is applied by solving a two-dimensional Schrödinger equation

$$\mathrm{i}\hbar \frac{\partial \psi(x, z, t)}{\partial t} = \left(\hat{T} + V(x, z) - \hat{\mu}(x, z) E_{\mathrm{pr}}(t)\right) \psi(x, z, t). \tag{53}$$

Here, $\hat{T}$ is the kinetic energy operator of the electron, $\hat{\mu}(x, z)$ the dipole operator, and $E_{\mathrm{pr}}(t)$ a Gaussian probe pulse. Figure 21(a) shows the initial wavepacket in coordinate space (x, z), figure 21(b) the (photoejected part of the) electron wavepacket after a sufficiently long propagation time, in momentum space (k_x, k_z).

From the initial and final wavepackets in coordinate and momentum space, the initial and final widths Δx_{ini} and Δk_{fin} can be derived, as detailed in [193]. By varying the width parameter σ_x of the solvation potential $V_{\mathrm{s}}(x, z)$, Δx_{ini} can systematically be varied. Figure 22 shows a

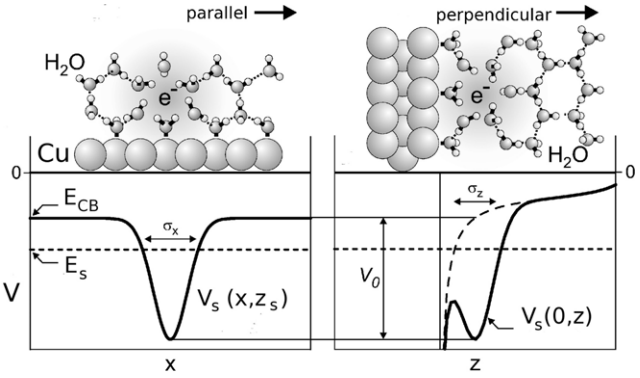

Figure 20. One-dimensional cuts through the localized electron potential, and illustration of the solvated electron. E_{CB} is the energy of the bottom of the conduction band of Cu(111), and E_{s} the energy of the solvated electron state, both relative to the vacuum level, E_{vac}.

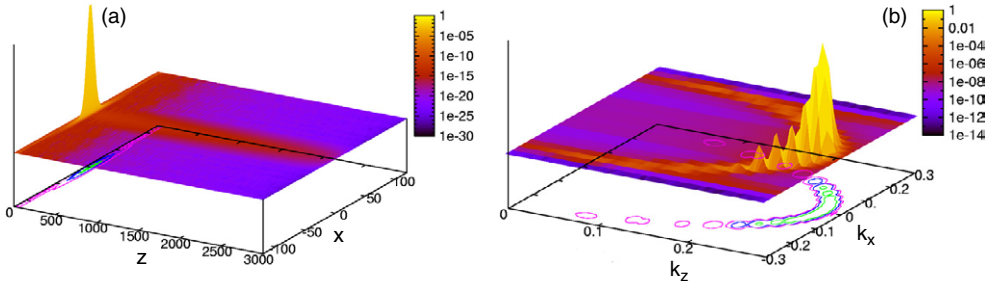

Figure 21. (a) Position space representation of the initial wavepacket, localized close to the surface. (b) Momentum space representation of the asymptotic part of the wavepacket at time $t_{\mathrm{fin}} = 200$ fs. The asymptotic part of the wavepacket is only about 1% of the total wavepacket. The potential parameters were $\sigma_x = 31.40a_0$ and $V_0 = 1.77$ eV. Shown are squared moduli of the wavepackets, $|\psi|^2$, in atomic units. Lengths and momenta are also given in atomic units.

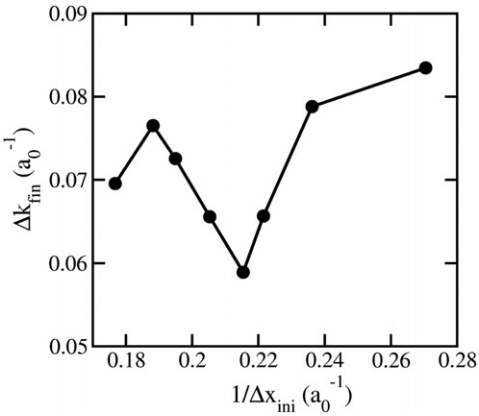

Figure 22. Dependence of the width Δk_{fin} of the ejected part of the final wavepacket in momentum space, on the width Δx_{ini} of the initial wavepacket in position space [193].

plot Δk_{fin} versus $1/\Delta x_{\mathrm{ini}}$, which should be a straight line according to equation (52). The figure demonstrates that the proportionality of Δk_{fin} to $1/\Delta x_{\mathrm{ini}}$ holds only approximately, hence

the quantitative extraction of the size of the wavepacket from AR-2PPE data is not entirely straightforward. The outgoing wavepacket carries not only information on the initial state, but also depends on transition dipole matrix elements, and on the density of final, unbound states, both of which are system dependent. These effects are not considered in equation (52).

For the present application, the pump step and the finite lifetime of the intermediate state were neglected, which is justified for the experiment modelled. Both effects can be important in other instances, however, for example for the calculation of TR-2PPE spectra of image potential states at metal surfaces [197]. In passing we note that the calculation of time- and energy-resolved 2PPE can also be done in a many-electron picture, so far albeit for model potentials only [198, 199].

5. Summary and conclusions

The desorption of atoms and molecules from surfaces is a key reaction in surface science. It can be enforced in various ways, ranging from simple surface heating, over direct excitation with light, with hot electrons, low energy electrons or holes from an STM, high energy electron beams, and other particles.

In this paper we have reviewed a few systems where nonadiabatic transitions lead to desorption and related phenomena. The focus was on our own work; however, closely related research by other groups was also mentioned. In particular, we presented results for H:Si(100)2×1, on (i) vibrational relaxation by vibration–phonon coupling, (ii) STM- and laser-induced desorption, and (iii) STM- and laser-induced H switching. Another system of interest was NO/Pt as a prototype for substrate mediated surface photochemistry, for which we worked towards (i) electronic lifetime calculations and (ii) the nuclear dynamics of photodesorption and its active control, using various models and strategies. We also considered CO on metal surfaces (Cu(100) and Ru(0001)), aiming at (i) vibrational lifetimes due to vibration–electron coupling, and (ii) ESD dynamics. The probing of ultrafast dynamics at surfaces by time-resolved spectroscopy was illustrated here by modelling two-pulse correlation traces (for NO/Pt), and two-photon-photoemission spectra (for solvated electrons in ice layers on Cu(111)).

In particular, this last example clearly demonstrates that electron dynamics matters, which has often been neglected so far. In fact, the time-limit of ultrafast processes is currently being pushed into the attosecond domain, also for surface science problems [200]. Attosecond processes define the natural timescale for electronic motion in atomic and molecular systems [201].

Another line of research aims at pushing the spatial resolution to the molecular limit. The keywords here are ‘molecular electronics’ and STM-induced ‘nanochemistry’. By an STM individual molecules can be manipulated. More generally, single-molecule research in combination with photochemistry holds promise, for example for light driven molecular switches [202].

In general, the active control of chemical reactivity at surfaces, by nanostructuring, incoherent, or coherent laser control, is a third actual direction of research. This is a challenge, as control in a dissipative environment is more difficult to achieve than in isolated systems.

Acknowledgments

We should like to express our thanks to several co-workers/colleagues, who contributed to the work covered in this paper: in alphabetical order, A Abe, R Baer, G Boendgen, W Brenig, C Corriol, G Darling, K Finger, R Kosloff, T Nakajima, L Pesce, S Holloway, K Yamashita, and M Wolf. We further thank V Staemmler (Bochum), to whom this paper is dedicated,

for enlightening discussions over the years on adsorption phenomena and quantum chemistry. We also gratefully acknowledge continuous support by the Deutsche Forschungsgemeinschaft (DFG) through the 'Sonderforschungsbereiche' SFB 450 and SFB 658, and through project Sa 547/7, and support by the 'Fonds der Chemischen Industrie'.

References

[1] Zimmermann F M and Ho W 1995 *Surf. Sci. Rep.* **22** 127
[2] Guo H, Saalfrank P and Seideman T 1999 *Prog. Surf. Sci.* **62** 239
[3] Tully J C 2000 *Annu. Rev. Phys. Chem.* **51** 153
[4] Camillone N III, Khan K A, Lasky P J, Wu L, Moryl J E and Osgood R M Jr 1998 *J. Chem. Phys.* **109** 8045
[5] Denzler D N, Frischkorn Ch, Hess C, Wolf M and Ertl G 2003 *Phys. Rev. Lett.* **91** 226102
[6] Bartels L, Wang F, Möller D, Knoesel E and Heinz T F 2004 *Science* **305** 648
[7] Stépán K, Güdde J and Höfer U 2005 *Phys. Rev. Lett.* **94** 236103
[8] Bonn M, Funk S, Hess C, Denzler D N, Stampfl C, Scheffler M, Wolf M and Ertl G 1999 *Science* **285** 1042
[9] Sauvage J-P 2001 *Molecular Machines and Motors* (Berlin: Springer)
[10] Huck N P M, Jager W F, de Lange B and Feringa B L 1996 *Science* **273** 1686
[11] Joachim C, Gimzewski J K and Aviram A 2000 *Nature* **408** 541
[12] Vondrak T and Zhu X-Y 1999 *Phys. Rev. Lett.* **82** 1967
[13] Buntin S A, Richter L J, Cavanagh R R and King D S 1988 *Phys. Rev. Lett.* **61** 1321
[14] Buntin S A, Richter L J, King D S and Cavanagh R R 1989 *J. Chem. Phys.* **91** 6429
[15] Budde F, Heinz T F, Loy M M T, Misewich J A, deRougemont F and Zacharias H 1991 *Phys. Rev. Lett.* **66** 3024
[16] Prybyla J A, Heinz T F, Misewich J A, Loy M M T and Glownia J H 1990 *Phys. Rev. Lett.* **64** 1537
[17] Misewich J A, Heinz T F and Newns D M 1992 *Phys. Rev. Lett.* **68** 3737
[18] Budde F, Heinz T F, Kalamarides A, Loy M M T and Misewich J A 1993 *Surf. Sci.* **283** 143
[19] Ho W 1996 *Surf. Sci.* **363** 166
[20] Prybyla J A, Tom H W K and Aumiller G D 1992 *Phys. Rev. Lett.* **68** 503
[21] Struck L M, Richter L J, Buntin S A, Cavanagh R R and Stephenson J C 1996 *Phys. Rev. Lett.* **77** 4576
[22] Misewich J A, Heinz T F, Weigand P and Kalamarides A 1995 *Laser Spectroscopy and Photochemistry on Metal Surfaces* ed H L Dai and W Ho (Singapore: World Scientific)
[23] Misewich J A, Nakabayashi S, Weigand P, Wolf M and Heinz T F 1996 *Surf. Sci.* **363** 204
[24] Kao F-J, Busch D G, Cohen D, Comes da Costa D and Ho W 1993 *Phys. Rev. Lett.* **71** 2094
[25] Busch D G and Ho W 1996 *Phys. Rev. Lett.* **77** 1338
[26] Shen T-C, Wang C, Abeln G C, Tucker J R, Lyding J W, Avouris Ph and Walkup R E 1995 *Science* **268** 1590
[27] Avouris Ph, Walkup R E, Rossi A R, Akpati H C, Nordlander P, Shen T-C, Abeln G C and Lyding J W 1996 *Surf. Sci.* **363** 368
[28] Persson B N J and Avouris Ph 1997 *Surf. Sci.* **390** 45
[29] Foley E T, Kam A F, Lyding J W and Avouris Ph 1998 *Phys. Rev. Lett.* **80** 1336
[30] Thirstrup C, Sakurai M, Nakayama T and Stokbro K 1999 *Surf. Sci.* **424** L329
[31] Quaade U J, Stokbro K, Thirstrup C and Grey F 1998 *Surf. Sci.* **415** L1037
[32] Stokbro K, Quaade U J, Lin R, Thirstrup C and Grey F 2000 *Faraday Discuss.* **117** 231
[33] Stipe B C, Rezaei M A and Ho W 1998 *Science* **280** 1732
Stipe B C, Rezaei M A and Ho W 1998 *Phys. Rev. Lett.* **81** 1263
Stipe B C, Rezaei M A and Ho W 1999 *Phys. Rev. Lett.* **82** 1724
[34] Bartels L, Meyer G and Rieder K-H 1997 *Phys. Rev. Lett.* **79** 697
[35] Stipe B C, Rezaei M A and Ho W 1998 *Science* **279** 1907
[36] Moresco F, Meyer G, Rieder K-H, Tang H, Gourdon A and Joachim Ch 2001 *Phys. Rev. Lett.* **87** 088302
[37] Dujardin G, Walkup R E and Avouris Ph 1992 *Science* **255** 1232
[38] Martel R, Avouris Ph and Lyo I-W 1996 *Science* **272** 385
[39] Stipe B C, Rezaei M A, Ho W, Gao S, Persson M and Lundquist B I 1997 *Phys. Rev. Lett.* **78** 4410
[40] Hla S W, Bartels L, Meyer G and Rieder K-H 2000 *Phys. Rev. Lett.* **85** 2777
[41] Pascual J I, Lorente N, Song Z, Conrad H and Rust H-P 2003 *Nature* **423** 525
[42] Wurm S, Feulner P and Menzel D 1995 *Phys. Rev. Lett.* **74** 2591
[43] Wurm S, Feulner P and Menzel D 1998 *Surf. Sci.* **400** 155
[44] See, for example: Polanyi J C and Williams R J 1988 *J. Chem. Phys.* **88** 3363
Mull T, Baumeister B, Menges M, Freund H-J, Weide D, Fischer C and Andresen P 1992 *J. Chem. Phys.* **96** 7108

Menges M, Baumeister B, Al-Shamery K, Freund H-J, Fischer C and Andresen P 1994 *J. Chem. Phys.* **101** 3318
Lu G Q, Linsbigler A and Yates J T Jr 1995 *J. Chem. Phys.* **102** 4657
Polanyi J C, Sze N S-K and Wang J-X 1997 *J. Phys. Chem.* A **101** 6679
Lu G Q, Linsbigler A and Yates J T Jr 1995 *J. Chem. Phys.* **102** 4657
Watanabe K, Takagi N and Matsumoto Y 2002 *Chem. Phys. Lett.* **366** 606
Dominguez-Ariza D, Lopez N, Illas F, Pacchioni G and Madey T E 2004 *Phys. Rev.* B **69** 075405 and references therein
[45] Anderson P W 1961 *Phys. Rev.* **124** 41
[46] Newns D M 1969 *Phys. Rev.* **178** 1123
[47] Gadzuk J W 1991 *Phys. Rev.* B **44** 13466
[48] Antoniewicz P R 1980 *Phys. Rev.* B **21** 3811
[49] Menzel D and Gomer R 1964 *J. Chem. Phys.* **41** 3311
Redhead P A 1964 *Can. J. Phys.* **42** 886
[50] Harris S, Holloway S and Darling G R 1995 *J. Chem. Phys.* **102** 8235
[51] Klamroth T, Kröner D and Saalfrank P 2005 *Phys. Rev.* B **72** 205407
[52] Saalfrank P 1995 *Chem. Phys.* **193** 119
[53] Whitten J L 2001 *J. Phys. Chem.* A **105** 7091
[54] Buenker R J, Liebermann H-P, Kokh D B, Izgorodina E I and Whitten J L 2003 *Chem. Phys.* **291** 115
[55] Kokh D B, Buenker R J, Liebermann H-P, Pichl L and Whitten J L 2005 *J. Phys. Chem.* B **109** 18070
[56] te Velde G and Baerends E J 1993 *Chem. Phys.* **177** 399
[57] Panas I, Siegbahn P and Wahlgren U 1988 *Theor. Chim. Acta* **74** 167
[58] Runge E and Gross E K U 1984 *Phys. Rev. Lett.* **52** 997
[59] Dominguez-Ariza D, Lopez N, Illas F, Pacchioni G and Madey T E 2004 *Phys. Rev.* B **69** 075405
[60] Besley N A 2005 *J. Chem. Phys.* **122** 184706
[61] van Dishoeck E F, van Hemert M C, Allison A C and Dalgarno A 1984 *J. Chem. Phys.* **81** 5709
[62] Baer M 1992 *Adv. Chem. Phys.* **82** 187
[63] Domcke W, Yarkony D R and Köppel H (ed) 2004 *Conical Intersections: Electronic Structure, Dynamics and Spectroscopy* (*Advanced Series in Physical Chemistry* vol 15) (New Jersey: World Scientific) and references therein
[64] Lindblad G 1976 *Commun. Math. Phys.* **48** 119
[65] Gorini V, Kossakowski A and Sudarshan E C G 1976 *J. Math. Phys.* **17** 821
[66] Alicki R and Lendi K 1987 *Quantum Dynamical Semigroups and Applications* (Berlin: Springer)
[67] Saalfrank P, Baer R and Kosloff R 1994 *Chem. Phys. Lett.* **230** 463
[68] Saalfrank P and Kosloff R 1996 *J. Chem. Phys.* **105** 2441
[69] Nest M and Saalfrank P 2000 *J. Chem. Phys.* **113** 8753
[70] Nest M and Saalfrank P 2001 *Chem. Phys.* **268** 65
[71] Nest M and Saalfrank P 2002 *J. Chem. Phys.* **116** 7189
[72] Gel'fand Y A and Likhtman E P 1971 *JETP Lett.* **13** 323
[73] Gao S 1997 *Phys. Rev. Lett.* **79** 3101
[74] Gao S 1998 *Phys. Rev.* B **57** 4509
[75] Gao S 1999 *Phys. Rev.* B **60** 15609
[76] Kaganov M I, Lifshitz I M and Tanatarov L V 1957 *Sov. Phys.—JETP* **4** 173
[77] Anisimov S I, Kapeliovich B L and Perel'man T L 1974 *Zh. Eksp. Teor. Fiz.* **66** 776
[78] Hohlfeld J, Wellershoff S-S, Güdde J, Conrad U, Jähnke V and Matthias E 2000 *Chem. Phys.* **251** 237
[79] Corkum P B, Brunel F, Sherman N K and Srinivasan-Rao T 1988 *Phys. Rev. Lett.* **61** 2886
[80] Berman M and Kosloff R 1991 *Comput. Phys. Commun.* **63** 1
[81] Pesce L and Saalfrank P 1998 *J. Chem. Phys.* **108** 3045
[82] Huisinga W, Pesce L, Kosloff R and Saalfrank P 1999 *J. Chem. Phys.* **110** 5538
[83] Dum R, Zoller P and Ritsch H 1992 *Phys. Rev.* A **45** 4879
[84] Dalibard J, Castin Y and Mølmer K 1992 *Phys. Rev. Lett.* **68** 580
[85] Mølmer K, Castin Y and Dalibard J 1993 *J. Opt. Soc. Am.* B **10** 524
[86] Andrianov I and Saalfrank P 2003 *Chem. Phys. Lett.* **367** 455
[87] Gadzuk J W, Richter L J, Buntin S A, King D S and Cavanagh R R 1990 *Surf. Sci.* **235** 317
[88] Gadzuk J W 1995 *Surf. Sci.* **342** 345
[89] Saalfrank P 1996 *Chem. Phys.* **211** 265
[90] Finger K and Saalfrank P 1997 *Chem. Phys. Lett.* **268** 291
[91] Saalfrank P, Boendgen G, Finger K and Pesce L 2000 *Chem. Phys.* **251** 51
[92] Gao S, Strömquist J and Lundquist B I 2001 *Phys. Rev. Lett.* **86** 1805

[93] Brandbyge M, Hedegård P, Heinz T F, Misewich J A and Newns D M 1995 *Phys. Rev.* B **52** 6042
[94] Fann W S, Storz R, Tom H W K and Bokor J 1992 *Phys. Rev. Lett.* **68** 2834
[95] Weik F, de Meijere A and Hasselbrink E 1993 *J. Chem. Phys.* **99** 682
[96] Knorren R, Bouzerar G and Bennemann K-H 2001 *Phys. Rev.* B **63** 094306
[97] Gao S, Lundquist B I and Ho W 1995 *Surf. Sci.* **341** L1031
[98] Tully J C, Gomez M and Head-Gordon M 1993 *J. Vac. Sci. Technol.* A **11** 1914
[99] Luntz A C and Persson M 2005 *J. Chem. Phys.* **123** 074704
[100] Springer C, Head-Gordon M and Tully J C 1994 *Surf. Sci.* **320** L57
[101] Springer C and Head-Gordon M 1996 *Chem. Phys.* **205** 73
[102] Gao S 1997 *Phys. Rev.* B **55** 1876
[103] Gao S, Busch D G and Ho W 1995 *Surf. Sci.* **344** L1252
[104] Persson B N J and Gadzuk J W 1998 *Surf. Sci.* **410** L779
[105] Chang H-C and Ewing G E 1990 *Phys. Rev. Lett.* **65** 2125
[106] Laß K, Han X and Hasselbrink E 2005 *J. Chem. Phys.* **123** 051102
[107] Morin M, Levinos N J and Harris A L 1992 *J. Chem. Phys.* **96** 3950
[108] Ashcroft N W and Mermin N D 1976 *Solid State Physics* (Orlando, FL: Holt, Rinehart and Winston)
[109] Guyot-Sionnest P, Lin P and Miller E 1995 *J. Chem. Phys.* **102** 4269
[110] Head-Gordon M and Tully J C 1992 *J. Chem. Phys.* **96** 3939
[111] Head-Gordon M and Tully J C 1992 *Phys. Rev.* B **46** 1853
[112] Persson B N J 1984 *J. Phys. C: Solid State Phys.* **17** 4741
[113] Corcelli S A and Tully J C 2002 *J. Phys. Chem.* A **106** 10849
[114] Andrianov I and Saalfrank P 2001 *Chem. Phys. Lett.* **350** 191
[115] Andrianov I and Saalfrank P 2006 *J. Chem. Phys.* **124** 034710
[116] Brenner D 1990 *Phys. Rev.* B **42** 9458
[117] Dyson A and Smith P 1999 *Mol. Phys.* **96** 1491
[118] Sbraccia C, Silvestrelli P and Ancilotto F 2002 *Surf. Sci.* **516** 147
[119] Persson B N J and Persson M 1980 *Solid State Commun.* **36** 175
[120] Hellsing B and Persson M 1984 *Phys. Scr.* **29** 360
[121] Trail J R, Graham M C, Bird D M, Persson M and Holloway S 2002 *Phys. Rev. Lett.* **88** 166802
[122] Trail J R, Bird D M, Persson M and Holloway S 2003 *J. Chem. Phys.* **119** 4539
[123] Mizielinski M S, Bird D M, Persson M and Holloway S 2005 *J. Chem. Phys.* **122** 084710
[124] Klamroth T and Saalfrank P 1998 *Surf. Sci.* **410** 21
[125] More W, Merino J, Monreal R, Pou P and Flores F 1998 *Phys. Rev.* B **58** 7385
[126] Taylor M and Nordlander P 2001 *Phys. Rev.* B **64** 115422
[127] Niedfeldt K, Carter E A and Nordlander P 2004 *J. Chem. Phys.* **121** 3751
[128] Borisov A G, Gauyacq J P, Kazansky A K, Chulkov E V, Silkin V M and Echenique P M 2001 *Phys. Rev. Lett.* **86** 488
[129] Borisov A G, Gauyacq J P, Chulkov E V, Silikin V M and Echenique P M 2002 *Phys. Rev.* B **65** 235434
[130] Sjakste J, Borisov A G and Gauyacq J P 2004 *Phys. Rev. Lett.* **92** 156101
[131] Bauer M, Pawlik S and Aeschlimann M 1997 *Phys. Rev.* B **55** 10040
[132] Ogawa S, Nagano H and Petek H 1999 *Phys. Rev. Lett.* **82** 1931
[133] Boendgen G and Saalfrank P 1998 *J. Phys. Chem.* B **102** 8029
[134] Saalfrank P, Boendgen G, Corriol C and Nakajima T 2000 *Faraday Discuss.* **117** 65
[135] Alavi S, Rousseau R and Seideman T 2000 *J. Chem. Phys.* **113** 4412
[136] Alavi S, Rousseau R, Lopinski G P, Wolkow R A and Seideman T 2000 *Faraday Discuss.* **117** 213
[137] Seideman T 2003 *J. Phys.: Condens. Matter* **15** R521
[138] Letokhov V S 1973 *Science* **180** 451
[139] Crim F F 1990 *Science* **249** 1387
[140] Shapiro M and Brumer P 1993 *J. Chem. Phys.* **98** 201
[141] Kopf A, Paramonov G K and Saalfrank P, unpublished
[142] Abe A, Yamashita K and Saalfrank P 2003 *Phys. Rev.* B **67** 235411
[143] Paramonov G K and Saalfrank P 1999 *Chem. Phys. Lett.* **301** 509
[144] Saalfrank P and Paramonov G K 1997 *J. Chem. Phys.* **107** 10723
[145] Paramonov G K and Saalfrank P 1999 *J. Chem. Phys.* **110** 6500
[146] Saalfrank P 1995 *Chem. Phys.* **193** 119
[147] Guo H and Liu L 1997 *Surf. Sci.* **372** 337
[148] Kühn O and May V 1996 *Chem. Phys.* **208** 117
[149] Howe P-T and Dai H-L 2000 *Surf. Sci.* **451** 12

[150] Saalfrank P 2000 *Int. J. Quantum Chem.* **80** 210
[151] Nest M and Saalfrank P 2004 *Phys. Rev.* B **69** 235405
[152] Nakagami K, Ohtsuki Y and Fujimura Y 2002 *Chem. Phys. Lett.* **360** 91
[153] Chakrabarti N, Balasubramanian V, Sathyamurthy N and Gadzuk J W 1995 *Chem. Phys. Lett.* **242** 490
[154] Abe A and Yamashita K 2003 *J. Chem. Phys.* **119** 9710
[155] Guo H 1997 *J. Chem. Phys.* **106** 1967
[156] Guo H and Ma G 2000 *Surf. Sci.* **451** 7
[157] Guo H and Chen F 1997 *Faraday Discuss.* **108** 309
[158] Chen F and Guo H 1998 *Chem. Phys. Lett.* **286** 205
[159] Li S and Guo H 2002 *J. Chem. Phys.* **117** 4499
[160] Zimmermann F M 1997 *Surf. Sci.* **390** 174
[161] Mull T, Baumeister B, Menges M, Freund H-J, Weide D, Fischer C and Andresen P 1992 *J. Chem. Phys.* **96** 7108
[162] Thiel S, Klüner T, Wilde M, Al-Shamery K and Freund H-J 1998 *Chem. Phys.* **228** 185
[163] Klüner T, Freund H-J, Freitag J and Staemmler V 1996 *J. Chem. Phys.* **104** 10030
[164] Klüner T, Freund H-J, Staemmler V and Kosloff R 1998 *Phys. Rev. Lett.* **80** 5208
[165] Klüner T, Thiel S, Freund H-J and Staemmler V 1998 *Chem. Phys. Lett.* **294** 413
[166] Bach C, Klüner T and Groß A 2003 *Chem. Phys. Lett.* **376** 424
[167] Bach C, Klüner T and Groß A 2004 *Appl. Phys.* A **78** 231
[168] Usman E Yu, Urazgil'din I F, Borisov A G and Gauyacq J P 2001 *Phys. Rev.* B **64** 205405
[169] Thumm U, Kürpick P and Wille U 2000 *Phys. Rev.* B **61** 3067
[170] Pesce L, Gerdts T, Manthe U and Saalfrank P 1998 *Chem. Phys. Lett.* **288** 383
[171] Gadzuk J W 2000 *Chem. Phys.* **251** 87
[172] Micha D A and Yi Z 1998 *Chem. Phys. Lett.* **298** 250
[173] Cai L, Xiao X and Loy M M T 2000 *Surf. Sci.* **464** L727
[174] Saalfrank P and Klamroth T 1995 *Ber. Bunsenges. Phys. Chem.* **99** 1347
[175] Menzel D 1969 *Surf. Sci.* **14** 340
[176] Xin Q-S and Zhu X-Y 1997 *Chem. Phys. Lett.* **265** 259
[177] Beyvers S, Ohtsuki Y and Saalfrank P 2006 submitted
[178] Eigler D M and Schweizer E K 1990 *Nature* **344** 524
[179] Stroscio J A and Eigler D M 1991 *Science* **254** 1319
[180] Eigler D M, Lutz C P and Rudge W E 1991 *Nature* **352** 600
[181] Ma G and Guo H 2000 *Chem. Phys. Lett.* **317** 315
[182] Corriol C, Darling G R, Holloway S, Brenig W, Andrianov I, Klamroth T and Saalfrank P 2002 *J. Chem. Phys.* **117** 4489
[183] Corriol C, Darling G R, Holloway S, Andrianov I, Klamroth T and Saalfrank P 2003 *Surf. Sci.* **528** 27
[184] Hilf M 1996 *Diploma Thesis* Technische Universität München
[185] Wolf M and Aeschlimann M 1998 *Phys. Bl.* **54** 145
[186] Petek H, Weida M J, Nagano H and Ogawa S 2000 *Science* **288** 1402
[187] Höfer U, Shumay I L, Reuß Ch, Thomann U, Wallauer W and Fauster Th 1997 *Science* **277** 1480
[188] Miller A D, Bezel I, Gaffney K J, Garrett-Roe S, Liu S H, Szymanski P and Harris C B 2002 *Science* **297** 1163
[189] Gahl C, Bovensiepen U, Frischkorn C and Wolf M 2002 *Phys. Rev. Lett.* **89** 107402
[190] Bovensiepen U, Gahl C and Wolf M 2003 *J. Phys. Chem.* B **107** 8706
[191] Ge N-H, Wong C M, Lingle R L Jr, McNeill J D, Gaffney K J and Harris C B 1998 *Science* **279** 202
[192] Bezel I, Gaffney K J, Garrett-Roe S, Liu S H, Miller A D, Szymanski P and Harris C B 2004 *J. Chem. Phys.* **120** 845
[193] Andrianov I, Klamroth T, Saalfrank P, Bovensiepen U, Gahl C and Wolf M 2005 *J. Chem. Phys.* **122** 234710
[194] Chulkov E V, Silkin V M and Echenique P M 1999 *Surf. Sci.* **437** 330
[195] Echenique P M, Pitarke J M, Chulkov E V and Rubio A 2000 *Chem. Phys.* **251** 1
[196] Harris C B, Ge N-H, Lingle R L Jr, McNeill J D and Wong C M 1997 *Annu. Rev. Phys. Chem.* **48** 711
[197] Klamroth T, Saalfrank P and Höfer U 2001 *Phys. Rev.* B **64** 035420
[198] Huber C and Klamroth T 2005 *Appl. Phys.* A **81** 93
[199] Saalfrank P, Klamroth T, Huber C and Krause P 2005 *Isr. J. Chem.* **45** 205
[200] Föhlisch A, Feulner P, Hennies F, Fink A, Menzel D, Sánchez-Portal D, Echenique P M and Wurth W 2005 *Nature* **463** 373
[201] Drescher M, Hentschel M, Kienberger R, Uiberacker M, Yakovlev V, Scrinzi A, Westerwalbesloh T, Kleineberg U, Heinzmann U and Krausz F 2002 *Nature* **419** 803
[202] Zhang C, Du M-H, Cheng H-P, Zhang X-G, Roitberg A E and Krause J L 2004 *Phys. Rev. Lett.* **92** 158301